The arabidopsis zinc finger proteins SRG2 and SRG3 are positive regulators of plant immunity and are differentially regulated by nitric oxide

New Phytologist

Research

The *Arabidopsis* zinc finger proteins SRG2 and SRG3 are positive regulators of plant immunity and are differentially regulated by nitric oxide

Beimi Cui[1,2,3,4], Shiwen Xu[1], Yuan Li[2], Saima Umbreen[2], Debra Frederickson[2], Bo Yuan[1,3], Jihong Jiang[1,3], Fengquan Liu[4], Qiaona Pan[1,2,3] and Gary J. Loake[2,3,5]

[1]The Key Laboratory of Biotechnology for Medicinal Plant of Jiangsu Province, School of Life Science, Jiangsu Normal University, Xuzhou 221116, China; [2]Institute of Molecular Plant Sciences, School of Biological Sciences, University of Edinburgh, Edinburgh, EH9 3BF, UK; [3]Transformational Centre for Biotechnology of Medicinal and Food Plants, Jiangsu Normal University – Edinburgh University, Xuzhou 221116, China; [4]Institute of Plant Protection, Jiangsu Academy of Agricultural Sciences, Nanjing 210014, China; [5]Centre for Synthetic and Systems Biology, School of Biological Sciences, University of Edinburgh, Edinburgh, EH9 3BF, UK

Authors for correspondence:
Qiaona Pan
Email: qiaona.pan@gmail.com

Gary J. Loake
Email: gloake@ed.ac.uk

Received: *13 March 2020*
Accepted: *25 September 2020*

New Phytologist (2020)
doi: 10.1111/nph.16993

Key words: *Arabidopsis thaliana*, disease resistance, nitric oxide, plant immunity, redox regulation, *S*-nitrosylation, zinc finger.

Summary

- Nitric oxide (NO) regulates the deployment of a phalanx of immune responses, chief among which is the activation of a constellation of defence-related genes. However, the underlying molecular mechanisms remain largely unknown. The *Arabidopsis thaliana* zinc finger transcription factor (ZF-TF), *S*-nitrosothiol (SNO) Regulated 1 (SRG1), is a central target of NO bioactivity during plant immunity. Here we characterize the remaining members of the *SRG* gene family.
- Both SRG2 and, especially, SRG3 were positive regulators of salicylic acid-dependent plant immunity. Analysis of *SRG* single, double and triple mutants implied that *SRG* family members have additive functions in plant immunity and, surprisingly, are under reciprocal regulation.
- SRG2 and SRG3 localized to the nucleus and functioned as ethylene-responsive element binding factor-associated amphiphilic repression (EAR) domain-dependent transcriptional repressors: NO abolished this activity for SRG3 but not for SRG2. Consistently, loss of GSNOR function, resulting in increased (S)NO concentrations, fully suppressed the disease resistance phenotype established from SRG3 but not SRG2 overexpression. Remarkably, SRG3 but not SRG2 was *S*-nitrosylated *in vitro* and *in vivo*.
- Our findings suggest that the *SRG* family has separable functions in plant immunity, and, surprisingly, these ZF-TFs exhibit reciprocal regulation. It is remarkable that, through neofunctionalization, the SRG family has evolved to become differentially regulated by the key immune-related redox cue, NO.

Introduction

A key feature upon attempted pathogen infection is the rapid production of the small, redox-active molecules nitric oxide (NO) and reactive oxygen species (ROS) (Grant & Loake, 2000; Gupta *et al.*, 2011; Yu *et al.*, 2014). NO, in particular, orchestrates a plethora of immune responses in plants, including salicylic acid (SA) biosynthesis and signalling (Feechan *et al.*, 2005; Tada *et al.*, 2008; Lindermayr *et al.*, 2010), phytoalexin accumulation (Delledonne *et al.*, 1998) and programmed cell death development (Delledonne *et al.*, 2001; Yun *et al.*, 2011).

The principal route for NO bioactivity is thought to be *S*-nitrosylation, the addition of a NO moiety to a cysteine (Cys) thiol to form an *S*-nitrosothiol (SNO) (Spadaro *et al.*, 2010; Astier *et al.*, 2011; Corpas & Barroso, 2014). Akin to other post-translational modifications (PTMs), *S*-nitrosylation can regulate protein structure, leading to modulation of protein activity (Wang *et al.*, 2009; Astier *et al.*, 2012; Mengel *et al.*, 2017; Zhan *et al.*, 2018) or localization (Tada *et al.*, 2008; Mengel *et al.*, 2013). S-nitrosoglutathione reductase (GSNOR) can turn over the natural NO donor, S-nitrosoglutathione (GSNO) (Feechan *et al.*, 2005; Lee *et al.*, 2008; Chen *et al.*, 2009), formed by the reaction of NO with glutathione (GSH), with GSNO acting as a reservoir of NO bioactivity (Corpas & Barroso, 2014). Thus, *GSNOR* loss-of-function mutants display increased GSNO concentrations and enhanced total cellular *S*-nitrosylation (Feechan *et al.*, 2005) and are impaired in multiple modes of plant immunity (Feechan *et al.*, 2005; Tada *et al.*, 2008) and also some developmental programmes (Kwon *et al.*, 2012). GSNOR RNA interference lines show similar phenotypes in tomato (Hussain *et al.*, 2019), suggesting the function of GSNOR is conserved across numerous dicotyledonous species.

In addition to the indirect SNO-reductase activity of GSNOR, Thioredoxin h5 may also function as a denitrosylase by directly reducing SNO groups present in some *S*-nitrosylated proteins (Kneeshaw *et al.*, 2014), providing an additional layer of regulation. Interestingly, NO and GSNO have also been shown to have separable and overlapping functions in the development of plant immunity, possibly because they redox-modulate the activity of different target proteins (Yun *et al.*, 2016).

The accumulating data suggest that NO production following the pathogen-triggered nitrosative burst contributes to the reprogramming of plant immune-response genes (Parani *et al.*, 2004; Zago *et al.*, 2006; Palmieri *et al.*, 2008; Bellin *et al.*, 2013; Xu *et al.*, 2013). However, the molecular mechanism(s) responsible remain largely opaque. To date, NO has been proposed to modulate the translocation of the transcriptional coactivator NPR1 into the nucleus (Tada *et al.*, 2008; Lindermayr *et al.*, 2010) and the specific DNA-binding activity of its protein interactor, the basic leucine-zipper transcription factor, TGA1 (Lindermayr *et al.*, 2010). Recently, the zinc finger transcription factor (ZF-TF), *SNO Regulated Gene 1* (*SRG1*), was shown to be a positive regulator of plant immune responses, by acting as a transcriptional repressor, presumably by suppressing the transcription of an immune repressor (Cui *et al.*, 2018). Significantly, SRG1 function during the plant immune response was shown to be modulated by *S*-nitrosylation of cysteine (Cys) 87, a highly evolutionary conserved residue, leading to both compromised DNA binding and, by extension, transcriptional repression activity.

Here we characterize the remaining members of the *SRG* gene family. Both SRG2 and, especially, SRG3 function as positive regulators of SA-dependent plant immunity. Genetic analysis of *SRG* single, double and triple mutants revealed that SRG family members have additive functions in plant immunity and, unexpectedly, are reciprocally regulated. Both SRG2 and SRG3 localized to the nucleus and acted as transcriptional repressors. Significantly, NO abolished this activity for SRG3 but not for SRG2. The absence of GSNOR function, leading to increased (S)NO concentrations, fully suppressed the disease resistance phenotype established from SRG3 overexpression but this was not found to be the case for overexpression of SRG2. SRG3 but not SRG2 was *S*-nitrosylated *in vitro* and *in vivo*, further highlighting the differences between these two SRG proteins. Our findings collectively suggest that the *SRG* family has separable functions in plant immunity and, surprisingly, these ZF-TFs exhibit reciprocal regulation. It is remarkable that through neofunctionalization the SRG family has evolved to become differentially regulated by the key immune-related redox cue, NO.

Materials and Methods

Plant materials

Arabidopsis thaliana (*Arabidopsis*) seeds were placed in ½ Murashige & Skoog (MS) medium, and subsequently 12-d-old plants were transferred to soil and grown at 22°C either under short-day conditions of 8 h : 16 h, light : dark (employed for pathogen infiltration experiments and quantitative PCR (qPCR) analysis) or under 16 h : 8 h, light : dark conditions (utilized for seed collection and plant transformation).

All plant genotypes including Col-0, *srg1* (SALK_119663), *srg2* (GABI_404D05), *srg3* (SAIL_1213_C07), *sid2-2* (Oide *et al.*, 2013) and *gsnor1-3*, were confirmed by PCR genotyping. The primers used are given in Supporting Information Table S1.

For the construction of *SRG2* or *SRG3* overexpression lines, the open reading frame (ORF) of *SRG2* or *SRG3* was fused to the CaMV*35S* promoter and C-terminal FLAG tag within the binary vector pGWB11 (Nakagawa *et al.*, 2007), employing the Gateway cloning system. To generate constructs for the conditional expression of either SRG2 or SRG3, the coding sequence of these genes was inserted into the *Xho*I/*Spe*I sites of the β-oestradiol-inducible vector pER8 (Zuo *et al.*, 2000). The resulting constructs were subsequently transferred into *Arabidopsis* Col-0 plants by *Agrobacterium*-mediated plant transformation (Clough & Bent, 1998; Zhang *et al.*, 2006). Plant transformants were confirmed by both antibiotic resistance and genotyping. To conditionally induce *SRG2*/ *SRG3* gene expression, 6-wk-old plants were sprayed with 100 μM β-oestradiol (Sigma) or dimethyl sulphoxide (DMSO; Invitrogen) and incubated for 48 h before further experiments.

The double mutant *srg2 srg3* was obtained by crossing the individual mutant lines. In a similar fashion, the *SRG2* and *SRG3* overexpression lines (*SRG2-OX* and *SRG3-OX*, respectively) were crossed with the *salicylic acid induction deficient* (*sid*) *2* and *gsnor1-3* mutants, employing the transgenic lines as pollen donors, to create the *SRG2-OX sid2-2*, *SRG3-OX sid2-2*, *SRG2-OX gsnor1-3* and *SRG3-OX gsnor1-3* lines. To generate the *srg1 srg2 srg3* triple mutant line, a *sgr1*-specific DNA sequence (14–34 bp) of the corresponding ORF was cloned into the CRISPR-Cas9 system vector pDe-CAS9 as previously described (Pyott *et al.*, 2016). The resulting construct was subsequently transformed into the *srg2 srg3* double mutant line by *Agrobacterium*-mediated transformation. Plants carrying the transgenic construct were selected in the T1 generation by spraying with a 120 mg l^{-1} solution of BASTA. The resulting transgenic plants were confirmed as *srg1 srg2 srg3* triple mutants by PCR genotyping.

Pathogen inoculation

The bacteria pathogen *Pseudomonas syringae* pv. *tomato* (*Pst*) DC3000 expressing the *avrRpm1* avirulence gene (*Pst* DC3000 (*avrRpm1*)) was cultured in low-salt LB medium (10 g l^{-1} tryptone, 5 g l^{-1} yeast extract and 5 g l^{-1} NaCl, pH 7.0) containing appropriate antibiotics and grown overnight in the dark at 28°C. Bacteria were collected by centrifugation and washed twice with 10 mM $MgCl_2$, then finally suspended in 10 mM $MgCl_2$ at a final concentration of 10^5 cells ml^{-1}. This bacterial solution was pressure-infiltrated into the leaves of 5-wk-old *Arabidopsis* plants of the indicated genotypes. At least 10 leaves from five different plants of a given genotype were inoculated for each experiment. Bacterial titres were determined at the time points indicated. The experiments were repeated at least three times.

Chemical treatments and histological staining

Ten-day-old seedlings or leaves from 5-wk-old plants were infiltrated with 1 μM flg22, 5 mM SA, 0.3 mM sodium nitroprusside (SNP) or 0.2 mM 2-(4-carboxyphenyl)-4,4,5,5-tetramethylimidazoline-1-oxyl-3-oxide (cPTIO) as required. Samples were subsequently collected at the indicated time points for qPCR assays. Mean values and SD were obtained from three biological replicates.

To assay cell death development, *Arabidopsis* leaves were stained using trypan blue (10 g phenol, 10 ml glycerol, 10 ml lactic acid, 10 ml water and 10 mg Trypan blue) by boiling for 2 min. Leaves were then destained with 2.5 g ml^{-1} chloral hydrate after cooling to room temperature. Images were taken following successful destaining. Subsequently, the relative intensity of staining was quantified by ImageJ (v.1.51j8, Java 1.8.0_261, Wayen Rasband, National Institutes of Health, Bethesda, MD, USA).

To explore the ROS burst, leaves were immersed in 0.5 mg ml^{-1} nitro blue tertrazolium (NBT; Sigma) for 3 h to detect superoxide formation or 1 mg ml^{-1} 3-3′-diaminobenzidine (DAB; Sigma) to score for hydrogen peroxide formation, for 8 h at room temperature in the dark. Following clearance of Chl, stained leaf discs were submerged in ethanol until clear and then photographed.

Quantification of cell death and ROS

Quantification of hydrogen peroxide was as previously described (Chen *et al.*, 2013) with minor modifications. Leaves were stained with freshly prepared 1 mg ml^{-1} DAB (Sigma) solution for 8 h, and Chl was then removed with ethanol. The resulting leaves were ground in liquid nitrogen after their weight was recorded and then solubilized in 0.2 M $HClO_4$, followed by centrifugation at 10 000 *g* for 15 min to remove debris. The absorbance of the resulting supernatants was measured immediately at A_{450} and quantified by comparison with a standard curve generated with known concentrations of H_2O_2 in 0.2 M $HClO_4$-DAB.

Quantification of superoxide was adapted as described previously (Chen *et al.*, 2013) with minor modifications. The leaf was stained with fresh NBT (0.5 mg ml^{-1}; Sigma) for 3 h, and then Chl was removed by addition of ethanol. The NBT-stained leaves were ground in liquid nitrogen, solubilized in 2 M KOH-DMSO, and then centrifuged at 10 000 ***g*** for 15 min to remove debris. The samples were evaluated at A_{630} and compared with a standard curve, generated with known amounts of NBT in the KOH-DMSO mix.

To measure electrolyte leakage induced by cell death, leaves from 5-wk-old plants were cut into 5-mm-diameter slices and soaked in water for 6 h, the conductivity of the solution was measured with a DiST WP conductivity meter (Hanna Instruments, Woonsocket, RI, USA) as previously described (Cui *et al.*, 2018). The units for this assay are microsvedbergs cm^{-1} (μS cm^{-1}), where the distance refers to that between the electrodes.

Reactive oxygen species production among wild-type Col-0 and mutant *Arabidopsis* plants was determined by luminol-based assay (Gómez-Gómez *et al.*, 1999; Smith & Heese, 2014). Leaves were cut into 5-mm-diameter slices and floated overnight on water. Subsequently, the water was removed and 0.1 ml of H_2O supplied containing 20 μM luminol, 1 μg horseradish peroxidase (Fluka, Gillingham, UK) and flg22 (Sigma) was added. Luminescence was measured in a Multimode Plate Reader SpectraMax M5 (Molecular Devices, Gillingham, UK) for 35 min; 1 μM flg22 was used in this experiment.

SA determination

Plant material (0.1 g) was collected and ground in liquid nitrogen. Samples were extracted using 95% ethanol and the resulting liquid was analysed by high-performance liquid chromatography-MS after centrifugation (Kim *et al.*, 2013).

Fluorescence microscopy and dual luciferase assays

For the localization of SRG2 and SRG3, the *SRG2* or *SRG3* ORFs were cloned into the binary vector pEarleyGate103, using the Gateway system, so their expression was driven by the CaMV*35S* promoter and a C-terminal green fluorescent protein (GFP) tag was added (Earley *et al.*, 2006). The truncation of the ethylene-responsive element binding factor-associated amphiphilic repression (EAR) motif of SRG proteins was undertaken utilizing a QuikChange II Site-Directed Mutagenesis Kit (Stratagene, Agilent Technologies, Cheadle, UK). The resulting constructs were transiently transformed into tobacco leaves or *Arabidopsis* protoplasts. A Leica TCS SP5 II confocal microscope was employed for GFP imaging (excitation 488 nm, emission 500–600 nm). Also, protein extracts were obtained from transformed leaves or protoplasts and subjected to Western blotting using an anti-GFP antibody (Sigma).

To score SRG2 and SRG3 for potential transcriptional repressive activity, 10 μl of the indicated DNA (4 μg of effector plasmid, 5 μg of reporter plasmid and 5 μg of internal plasmid) was transformed into *Arabidopsis* protoplasts and incubated for 16 h. The resulting cells were then collected and extracted for luciferase activity assay using a Dual-Luciferase Report Assay System (Promega) with a SpectraMax M5 Multimode Plate Reader (Molecular Devices). Ten replicates were measured for each experiment. Each experiment was repeated at least three times.

qPCR

Total RNA was extracted from 0.1 g plant tissue using a RNA isolation mini-kit (Agilent Technologies) and cDNA was synthesized from 2 μg total RNA employing oligo (dT) primers and reverse transcriptase (First-Strand cDNA Synthesis Kit; Invitrogen). PCR was performed in a 20 μl reaction containing SYBR Green PCR Master Mix (Applied Biosystems, Foster City, CA, USA), cDNA and primers (listed in Table S1) utilizing the LightCycler® 480 Real-Time PCR System (Roche). *UBQ10* and

UBC9 were used as internal controls. Mean values and standard deviations were obtained from at least three biological replicates.

Protein expression and S-nitrosylation

The ORFs of either *SRG2* or *SRG3* were cloned into the expression vector pMAL-c5X with a maltose-binding protein (MBP) tag at the N-terminus. The construct was transformed into *Escherichia coli* strain *BL21*(DE3) for protein expression, then purified using amylose magnetic beads (New England Biolabs, Ipswich, MA, USA). The purified protein was utilized for further experiments.

S-nitrosylation assays employing purified recombinant protein or proteins extracted directly from plant tissue were interrogated by the biotin switch assay (BSA) (Jaffrey & Snyder, 2001). CysNO was synthesized by dissolving 13 mg of reduced free L-cysteine in 0.5 ml of 0.1 M HCl, and then added to 0.5 ml of 220 mM $NaNO_2$ to obtain 110 mM CysNO. The CysNO was maintained in the dark for 20 min and then diluted to working concentration. Freshly prepared CysNO was always utilized in any experiments performed.

Statistics

Data are expressed as means ± SD from a minimum of three independent experiments. Statistical analysis of the data was carried out using ANOVA analysis followed by Dunnett's test unless otherwise specified. Differences were considered significant at $P < 0.05$ (*) and highly significant at $P < 0.01$ (**).

Results

The expression of *SRG1* homologues, *SRG2* and *SRG3*, are induced by pathogens and NO

Previously we identified an *Arabidopsis* C2H2 type ZF-TF, SRG1, which positively regulates plant immunity (Cui *et al.*, 2018). SRG1 function is regulated at the transcriptional and post-transcriptional level by NO (Cui *et al.*, 2018). Phylogenetic analysis showed that four C2H2-type ZF-TFs were classified into a small group: *SRG1*, *SRG2* (*At3g46090*), *SRG3* (*At5g59820*) and *SRG4* (*At3g46070*) (Fig. S1a). In order to examine whether these *Arabidopsis* SRG1 paralogues are also involved in plant immunity, quantitative reverse transcription polymerase chain reaction (qRT-PCR) was performed to determine if the expression of these genes was transcriptionally activated by the plant immune activator SA, flg22, a pathogen-associated molecular pattern (PAMP) derived from bacterial flagellin or *Pst* DC3000, a virulent bacterial pathogen on the Col-0 accession of *Arabidopsis* (Whalen *et al.*, 1991). Expression of *SRG2* and *SRG3* was induced by all three of these immune-related stimuli (Figs 1a–d, S1b,c), implying that these genes might participate in the establishment of plant immunity. By contrast, transcripts of *SRG4* did not accumulate in response to these cues (Fig. S1d), so this gene was not investigated further. Interestingly, the expression of both *SRG2* and *SRG3* could also be induced by the NO donors, SNP and GSNO (Figs 1e,f, S1e–i). Either SNP- or GSNO-induced *SRG3* expression was also significantly reduced in the presence of the NO scavenger, cPTIO. Conversely, SNP- and GSNO-induced *SRG2* expression was only weakly reduced by this NO scavenger (Figs 1e,f, S1g). Thus, while *SRG3* expression is responsive to NO, the accumulation of *SRG2* transcripts appears to be strikingly less sensitive to this redox signalling cue.

Constitutive expression of *SRG2* and *SRG3* enhances plant immunity

To gain further insights into the possible role(s) of *SRG2* and *SRG3* in plant immunity, plants containing *35S::SRG2-FLAG* (*SRG2-OX*) or *35S::SRG3-FLAG* (*SRG3-OX*) transgenes were generated. These transgenic lines exhibited reduced stature compared with wild-type Col-0 (Fig. 2a,b). Further, the FW of these lines was directly correlated with the strength of *SRG2* or *SRG3* expression (Fig. 2c–f). Thus, *SRG2* and *SRG3* expression negatively impacts *Arabidopsis* stature.

To examine the effect of SRG2 and SRG3 on basal immunity, *Pst* DC3000 was inoculated into *SRG2-OX* and *SRG3-OX* transgenic plants and the bacterial titre determined over time. The amount of infiltrated *Pst* DC3000 in the *SRG2-OX* and *SRG3-OX* transgenic lines was comparable to wild-type Col-0 at 0 d post-inoculation (dpi) (Fig. 2g,h), which suggests that *SRG2-OX* and *SRG3-OX* transgenic plants can be infiltrated to similar extents as the wild-type. Hence, *SRG2* and *SRG3* overexpression does not reduce the amount of infiltrated bacteria. A reduced titre of *Pst* DC3000 was detected in *SRG2-OX* and *SRG3-OX* transgenic plants compared with the wild-type at 3 dpi (Fig. 2g,h). Further, our data suggest that the level of *SRG2* and *SRG3* expression is directly related to the extent of resistance against *Pst* DC3000, demonstrating that *SRG2* and *SRG3* act as positive regulators of plant basal disease resistance.

We next examined the impact of *SRG2* and *SRG3* expression on *R* gene-mediated disease resistance. *Pst* DC3000 expressing the avirulence gene *avrRpm1* (*Pst* DC3000(*avrRpm1*)) is recognized by the R protein, RPM1, in the Col-0 accession of *Arabidopsis* (Grant *et al.*, 1995). The titre of *Pst* DC3000 (*avrRpm1*) in *SRG-OX* plants was significantly less than that in the wild-type at 3 dpi (Fig. 2i,j), indicating that overexpression of *SRG2* or *SRG3* leads to increased resistance against *Pst* DC3000 (*avrRpm1*). These results imply that overexpression of *SRG2* or *SRG3* in *Arabidopsis* enhances both basal defence and *R* gene-mediated resistance. Collectively, our findings therefore suggest that *SRG2* and *SRG3* are positive regulators of plant immunity.

SRG2 and *SRG3* overexpression lines exhibit elevated cell death, accumulation of ROS and constitutive *PR1* expression

High levels of *SRG2* and *SRG3* overexpression resulted in the formation of microlesions, which was confirmed by trypan blue (TB) staining and associated microscopy (Fig. 3a). The relative intensity of cell death staining was quantified by ImageJ, which indicated that microlesion formation increased with increasing

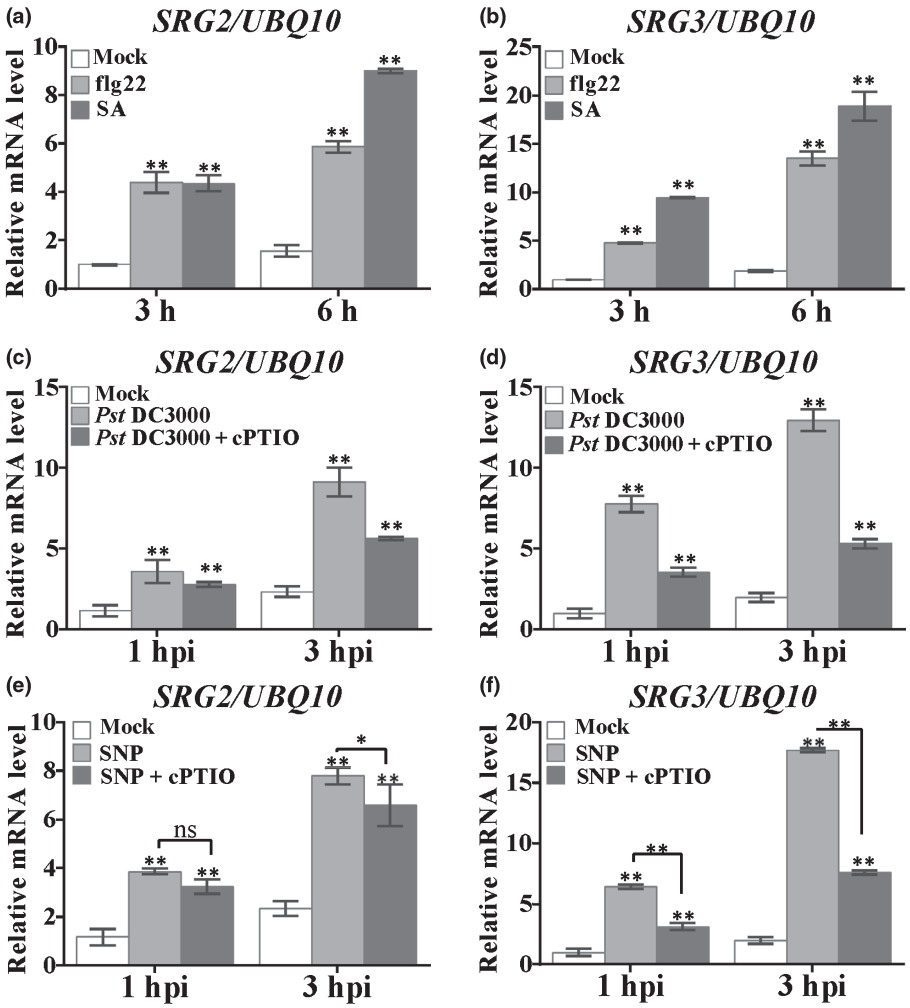

Fig. 1 Expression of *Arabidopsis SRG2* and *SRG3* is nitric oxide- and pathogen-inducible. (a, b, e, f) Relative gene expression of *SRG2* (a, e) and *SRG3* (b, f) in response to flg22, salicylic acid (SA), sodium nitroprusside (SNP) or SNP with 2-(4-carboxyphenyl)-4,4,5,5-tetramethylimidazoline-1-oxyl- 3-oxide (cPTIO) treatment. Ten-day-old seedlings were used for these experiments and water was employed as a control. *UBQ10* was utilized as an internal control. Error bars represent means ± SD. hpi, h post-inoculation. (c, d) Transcript abundances of *SRG2* (c) and *SRG3* (d) were determined following treatment with *Pseudomonas syringae* pv. *tomato* (*Pst*) DC3000 or *Pst* DC3000 + cPTIO. *UBQ10* was utilized as an internal control. Experiments were repeated at least three times. Error bars represent means ± SD. One-way ANOVA assays were performed to determine significant differences relative to mock treatments or indicated lines, **, $P < 0.01$; *, $P < 0.05$; ns, not significant.

SRG2 or *SRG3* expression (Fig. 3b). Thus, *SRG2-OX#2* and *SRG3-OX#2* lines exhibited increased cell death relative to *SRG2-OX#1* and *SRG3-OX#1* lines (Fig. 3b). The formation of these microlesions did not occur within cotyledons and did not appear to be temperature-dependent.

ROS formation is a key early defence response (Grant & Loake, 2000; Torres *et al.*, 2006). Therefore, we treated the leaves of *SRG2-OX* and *SRG3-OX* lines with either DAB, which stains hydrogen peroxide (H_2O_2), or NBT, which stains superoxide (O_2^-) (Jabs *et al.*, 1996; Thordal-Christensen *et al.*, 1997; Grant *et al.*, 2000), to determine potential accumulation of these molecules. Both *SRG2-OX* and *SRG3-OX* lines exhibited increased DAB and NBT staining compared with that of wild-type Col-0 (Fig. 3c–f). Further, increasing *SRG2* or *SRG3* expression resulted in enhanced DAB and NBT staining (Fig. 3d,f). We also determined the expression of the SA marker gene, *Pathogenesis-Related1* (*PR1*). As expected, *PR1* expression was significantly increased in *SRG2-OX* and *SRG3-OX* lines compared with wild-type Col-0 (Fig. 3g) and was positively correlated to *SRG* transcript accumulation. Taken together, our results show that overexpression of *SRG2* or *SRG3* activates a number of immune responses, including cell death development, ROS production and *PR1* expression.

SRG2 and *SRG3* promote increased basal and *R* gene-mediated immunity

To further investigate the biological contribution of *SRG2* and *SRG3* in plant immunity, T-DNA insertion lines for these genes were obtained and homozygous loss-of-function mutants generated utilizing PCR genotyping (Fig. S2a). The expression level of *SRG1*, *SRG2* and *SRG3* in these T-DNA loss-of-function

New Phytologist

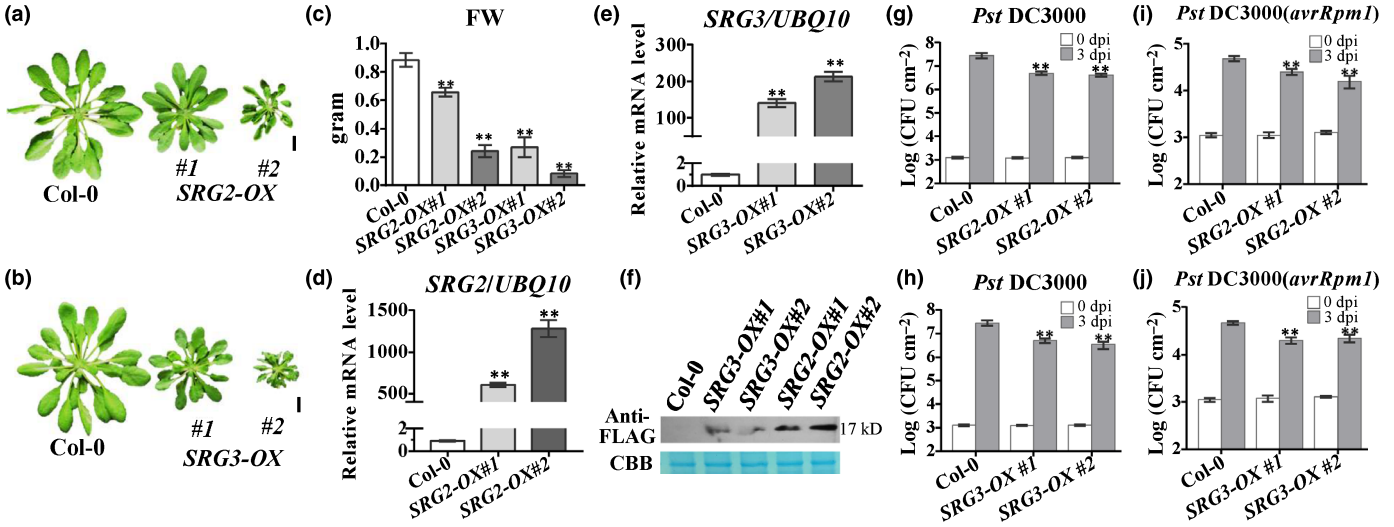

Fig. 2 Either *SRG2* or *SRG3* overexpression in *Arabidopsis* enhances pathogen resistance. (a–c) Morphological phenotype (a, b) and FW measurements (c) of 6-wk-old *SRG* overexpression (*SRG-OX*) lines and Col-0 under short-day conditions (8 h : 16 h, light : dark). Bars, 1 cm. Error bars indicate means ± SD ($n \geq 5$). **, $P < 0.01$. (d, e) mRNA level of *SRG2* (d) and *SRG3* (e) in the stated *Arabidopsis* lines. Error bars indicate means ± SD from three to six biological replicates. **, $P < 0.01$. (f) Western blot analysis of either SRG2 or SRG3 protein expression in *SRG* overexpression lines using an anti-FLAG antibody. Total protein extracted from fresh leaves of indicated lines was used in these experiments. Wild-type Col-0 plants served as negative controls. Coomassie Brilliant Blue (CBB) stain was employed as loading control. (g–j) Bacterial titre of *Pseudomonas syringae* pv. *tomato* (*Pst*) DC3000 (g, h) and *Pst* DC3000 carrying *avrRpm1* (i, j) in the indicated plant genotypes. Error bar indicates mean ± SD ($n = 7$). One-way ANOVA assay: **, $P < 0.01$. All experiments were repeated at least three times.

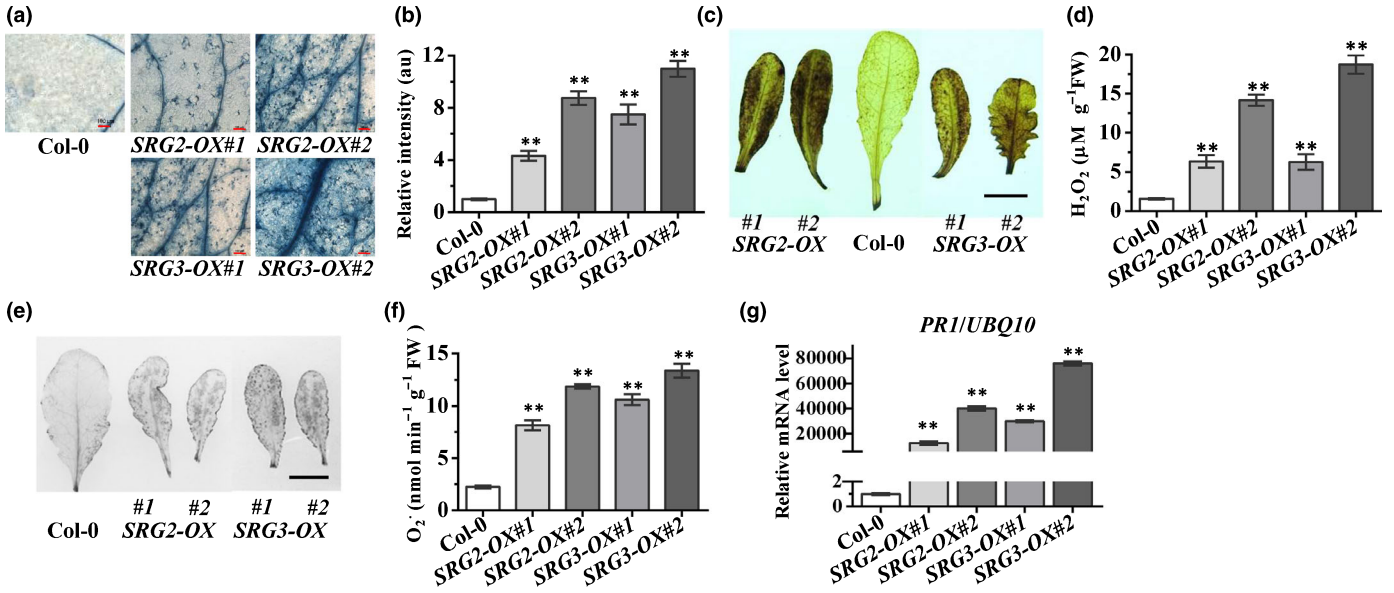

Fig. 3 Both *SRG2* and *SRG3* overexpression promotes activation of *Arabidopsis* key defence responses. (a) Cell death development was scored by trypan blue (TB) staining. Leaves from 6-wk-old plants were stained and observed by microscopy. Bars, 100 μm. (b) The relative intensity of TB staining was performed with ImageJ software. Error bars indicate means ± SD, $n \geq 10$. **, $P < 0.01$. (c) Accumulation of H_2O_2 in 6-wk-old plant leaves was determined by 3,3′-diaminobenzidine (DAB) staining. Bar, 5 mm. (d) Quantification of H_2O_2 in 10-d-old *Arabidopsis* seedlings of the indicated genotypes; 0.1 g of seedlings from each line were grouped as one sample. Error bars indicate ± SD ($n = 5$). **, $P < 0.01$. (e) Accumulation of superoxide in 6-wk-old plant leaves was detected by nitro blue tetrazolium (NBT) staining. Bar, 5 mm. (f) Quantification of superoxide production in 10-d-old seedlings of the indicated genotypes. Error bars indicate ± SD ($n = 5$). **, $P < 0.01$. (g) mRNA level of *PR1* in the stated *Arabidopsis* lines. Error bars indicate means ± SD. Experiments were repeated three times with similar results. **, $P < 0.01$.

insertion lines was determined by qPCR, which confirmed that these lines were null mutants for the relevant genes and also indicated a complex transcriptional relationship among them (Fig. 4a). Surprisingly, loss-of-function mutations in either *SRG1* or *SRG3* strikingly reduced *SRG2* expression. *SRG3* expression, by contrast, was not reduced in loss-of-function *srg1* plants and was only reduced by *c.* 30% in a loss-of-function *srg2* line. *SRG1* transcript accumulation was reduced *c.* 60 % in either *srg2* or *srg3*

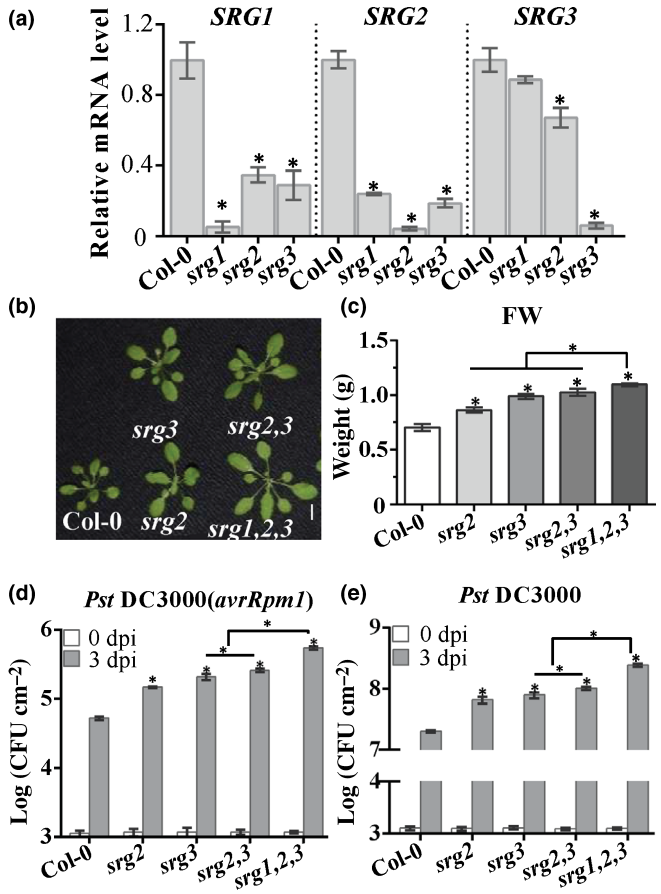

Fig. 4 *SRG2* and *SRG3* are required for *Arabidopsis* immunity. (a) Transcript abundances of *SRG2*, *SRG3* and *SRG1* in the given plant lines. Error bars indicate mean ± SD. Experiments were repeated three times with similar results. *, $P < 0.05$. (b) Growth status of indicated plant genotypes at 4 wk old under 8 h : 16 h, light : dark conditions. Bar, 1 cm. (c) FW quantification of the indicated plant lines at 5 wk. Error bars represent means ± SD ($n \geq 5$). *, $P < 0.05$. (d, e) Titre of *Pseudomonas syringae* pv. *tomato* (*Pst*) DC3000(*avrRpm1*) (d) and *Pst* DC3000 (e) in the indicated plant genotypes. Error bars indicate ± SD ($n = 7$). *, $P < 0.05$. All experiments were repeated at least three times.

loss-of-function mutants. These three ZF-TFs are therefore under reciprocal regulation. The expression of *SRG* genes in the *SRG* overexpression lines also revealed a complex relationship between these transcription factors (Fig. S2b).

Of these C2H2 ZF TFs, *SRG2*, *SRG3* and *SRG1* share high similarities in DNA sequence and might function redundantly. Therefore, a *srg2 srg3* double loss-of-function mutant was obtained by crossing the associated single mutations, followed by PCR analysis of F_2 plants. We also generated a *srg1 srg2 srg3* triple loss-of-function mutant. As *SRG1* and *SRG2* are closely linked, we employed CRISPR/Cas9 gene editing technology to mutate *SRG1* in a *srg2 srg3* double mutant. Interestingly, phenotypic analysis indicated there was a small increase of FW in the *srg1*, *srg2* and *srg3* single *SRG* loss-of-function mutants compared with that of the wild-type and a significant increase in FW in the triple loss-of-function mutant (Fig. 4b,c). Thus, loss-of-function mutations in *SRG1*, *SRG2* and *SRG3* exhibit partially overlapping impacts on *Arabidopsis* growth. The expression of these ZF-TFs was then determined in the associated double and triple mutants (Fig. S2c–e). *SRG2* expression was abolished in the *srg2 srg3* double mutant and in the *srg1 srg2 srg3* triple loss-of-function mutant. In a similar fashion, *SRG3* expression was abolished in the *srg2 srg3* double loss-of-function mutant and the *srg1 srg2 srg3* triple loss-of-function mutant.

To examine if *SRG2*, *SRG3* and *SRG1* have redundant functions in plant immunity, *Pst* DC3000 (*avrRpm1*) was infiltrated into the associated loss-of-function mutants and the bacterial titre was recorded over time (Fig. 4d). Both single loss-of-function mutants support more *Pst* DC3000(*avrRpm1*) compared with wild-type Col-0 and the titre in the *srg2 srg3* loss-of-function line was significantly higher than that in the respective single loss-of-function mutants, indicating disruption of *SRG2* or *SRG3* leads to an increased titre of *Pst* DC3000(*avrRpm1*). Significantly, statistical analysis revealed that the titre of *Pst*DC3000(*avrRpm1*) in the *srg1 srg2 srg3* triple loss-of-function mutant is significantly higher than that in the *srg2 srg3* double mutant and *srg1*, *srg2* and *srg3* single loss-of-function mutants. Also, the *srg2 srg3* double mutant is more susceptible than *srg2* and *srg3* single loss-of-function mutants. The impact of these mutations on basal disease resistance was tested. Similar results were observed following inoculation of *Pst* DC3000 (Fig. 4e).

Taken together, our findings suggest that *SRG1*, *SRG2* and *SRG3* are required for *R* gene-mediated protection and basal resistance and there is functional redundancy between these ZF-TFs.

Loss of *SRG2*, *SRG3* and *SRG2 SRG3* function reduces cell death development, ROS production and SA accumulation

As *SRG2-OX* and *SRG3-OX* lines exhibited elevated cell death development, we assessed the biological consequence of a loss of either *SRG2* or *SRG3* function on development of the hypersensitive response (HR) during the development of immunity. Leaves were stained by TB after *Pst* DC3000(*avrRpm1*) infiltration, and TB staining was then quantified. Cell death development was diminished in these mutants relative to wild-type Col-0 at 12 h post-inoculation (hpi; Fig. S3a,b). Further, this result was confirmed by transient overexpression of either *SRG2* or *SRG3* in the respective *SRG* loss-of-function lines using an β-estradiol-inducible expression system (Zuo *et al.*, 2000) (Fig. S3c,d). β-estradiol-treated plants showed higher *SRG2* or *SRG3* expression respectively and increased TB staining in leaves, whereas mock treatment did not induce either *SRG2* or *SRG3* expression, and cell death development was similar to that scored in the *srg2* and *srg3* loss-of-function mutants (Fig. S3c,d). To further determine the extent of HR cell death in these lines, electrolyte leakage was quantified (Fig. 5a,b). Again, the amount of electrolyte leakage was reduced in these single, double and triple *SRG* loss-of-function mutants compared with wild-type Col-0, with that in the *srg1 srg2 srg3* triple loss-of-function mutant most pronounced (Fig. 5a), implying that *SRG2*, *SRG3* and *SRG1* play important roles in HR development during immunity. Further, we examined the effects of transient conditional *SRG2* or *SRG3* overexpression in *srg2* or *srg3* loss-of-function lines, respectively, on

electrolyte leakage. Following challenge with *Pst* DC3000 (*avrRpm1*), β-estradiol cued *SRG2* or *SRG3* transient overexpression resulted in higher electrolyte leakage relative to mock-treated plants (Fig. 5b).

We determined ROS production upon *Pst* DC3000 challenge in the single, double and triple *SRG* loss-of-function mutants by a luminol-based assay (Gómez-Gómez *et al.*, 1999). ROS production was slightly reduced in *srg1*, *srg2 and srg3* single loss-of-function mutants and also the *srg2 srg3* double loss-of-function mutant in response to *Pst* DC3000 (Fig. 5c). Statistical analysis showed that total ROS accumulation was significantly reduced in the *srg1 srg2 srg3* triple loss-of-function mutant compared with the related double or single loss-of-function mutants (Fig. S3d). Further, we used flg22 to examine PAMP-induced ROS production in these lines. The ROS burst was faster and stronger in wild-type Col-0 after treatment with flg22, whereas it was reduced in the related double and triple loss-of-function mutants (Figs 5d, S3e). Further, the *srg1 srg2 srg3* triple loss-of-function mutant exhibited reduced total ROS production following flg22 treatment relative to the *srg1*, *srg2*, *srg3* single loss-of-function mutants. Moreover, increased ROS accumulation was observed following conditional transient overexpression of either *SRG2* or *SRG3* relative to the mock control (Figs 5e, S3f).

Overexpression of either *SRG2* or *SRG3* induced *Respiratory Burst Oxidase Homolog D* (*RBOHD*) expression, which encodes the key source of pathogen-triggered apoplastic ROS (Grant & Loake, 2000; Torres *et al.*, 2006) (Fig. S3g). Together, these results further support the suggestion that *SRG2*, *SRG3* and *SRG1* play important and redundant functions required for immune-related ROS production.

We also examined the expression of the SA-associated marker, *PR1*, in response to inoculation of *Pst* DC3000 (Fig. 6a). Compared with the wild-type, *PR1* expression was reduced in all *SRG* loss-of-function mutants. However, the *srg2 srg3* double loss-of-function mutant exhibited a reduction greater than that in the single *srg1*, *srg2* and *srg3* loss-of-function mutants, and the triple *srg1 srg2 srg3* loss-of-function mutant showed lower *PR1* expression than the double mutant at both 12 and 24 hpi. Further, SA concentrations in these lines were also analysed upon *Pst* DC3000 infection. The concentration of SA was similar in all tested plant lines without infection (Fig. 6b), suggesting that the size of *srg* mutants may not be associated with SA accumulation. A significant increase of SA in wild-type Col-0 plants was observed upon pathogen inoculation at both 12 and 24 hpi, whereas SA concentration in the single, double and triple *SRG* loss-of-function mutants, especially the triple mutant, was significantly decreased compared with wild-type Col-0 (Fig. 6b), linking the pathogen susceptibility of these *SRG* loss-of-function mutants to a decrease in SA accumulation. Therefore, we also determined the expression level of *CBP60g*, *SARD1* and *WRKY62* genes implicated in the regulation of SA synthesis in this collection of mutant lines in response to *Pst* DC3000 inoculation. Expression of *CBP60g*, *SARD1* and *WRKY62* was reduced upon *Pst* DC3000 infection in all of these mutants and this was especially pronounced in the *srg1 srg2 srg3* triple loss-of-function mutant (Fig. S4), further implicating *SRG2*, *SRG3* and *SRG1* in

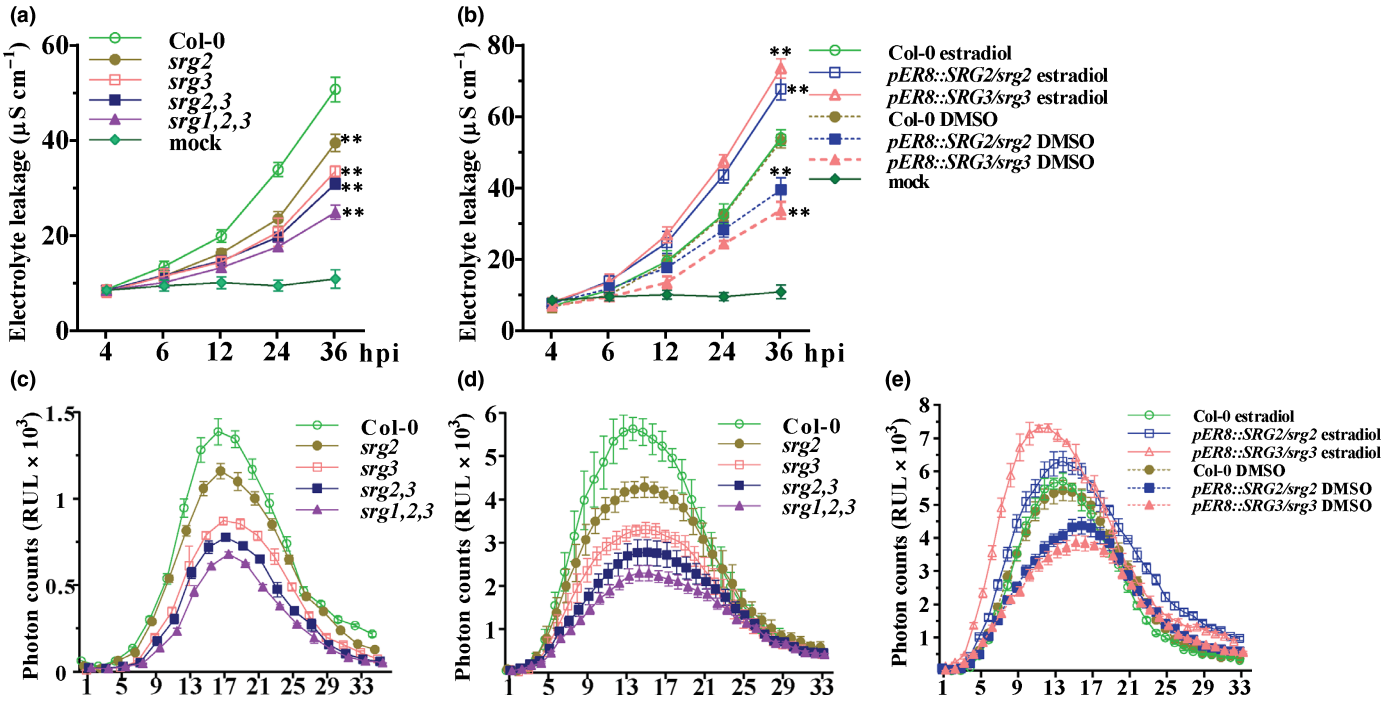

Fig. 5 Loss of *SRG2* and *SRG3* function reduces both cell death development and accumulation of reactive oxygen species (ROS) in *Arabidopsis*. (a, b) Electrolyte leakage triggered by *Pseudomonas syringae* pv. *tomato* (*Pst*) DC3000 in the indicated lines was measured with a conductivity meter. Error bars indicate means ± SD ($n = 8$). One-way ANOVA assays were performed to determine significant differences at 36 h post-inoculation (hpi) relative to wild-type Col-0 (a) or wild-type Col-0 dimethyl sulphoxide (DMSO) (b). **, $P < 0.01$. (c–e) ROS production in response to *Pst* DC3000 (c) or flg22 (d, e) treatment was determined by a luminol-based assay. Error bars indicate means ± SD ($n = 6$).

SA-associated immune responses. We also crossed our *SRG2-OX* and *SRG3-OX* lines with the SA biosynthesis-deficient mutant, *salicylic acid induction deficient 2-2* (*sid2-2*) (Oide *et al.*, 2013). In *SRG2-OX sid2-2* and *SRG3-OX sid2-2* lines the reduced physical stature resulting from overexpression of either *SRG2* or *SRG3* was only partially recovered (Fig. 6c,d), implying that the impact of either *SRG2* or *SRG3* overexpression on *Arabidopsis* growth is not totally dependent on SA accumulation. However, the titre of *Pst*DC3000 in either *SRG2-OX sid2-2* or *SRG3-OX sid2-2* lines was similar to that in wild-type Col-0 plants (Fig. 6e,f). Similar results were observed following inoculation of *Pst* DC3000 (*avrRpm1*) (Fig. 6g,h). Collectively, these results suggest that *SRG2* and *SRG3* regulate plant immunity through the SA pathway.

SRG2 and *SRG3* encode NO-regulated transcriptional repressors

SRG2 and SRG3 are plant C2H2 ZF TFs containing a predicted nuclear localization signal (NLS) (Fig. 7a). To test the functionality of this domain, *SRG2* and *SRG3* were fused to the C-terminus of GFP downstream of the CaMV*35S* promoter. Each of the resulting constructs was then transiently transformed into tobacco leaves (Fig. S5a) or *Arabidopsis* protoplast (Fig. S5c). The integrity of each of these fusion proteins was confirmed by Western blot analysis (Fig. S5b,d). In both tobacco and *Arabidopsis*, SRG2-GFP and SRG3-GFP localized to the nucleus.

Similar to SRG1, SRG2 and SRG3 both contain a leucine-rich EAR motif-like sequence within their C-terminus (Fig. 7a). This motif has previously been reported to function as a transcriptional repressor (Kagale & Rozwadowski, 2011; Cui *et al.*, 2018). Therefore, we carried out a transcriptional activity assay in *Arabidopsis* protoplasts with either a *Galactose 4 DNA Binding Domain* fused with either *SRG2* or *SRG3* (*GAL4-DB-SRG2* or *GAL4-DB-SRG3*, respectively) together with a reporter gene comprising five copies of the *GAL4 DNA*-binding site fused to the firefly *Luciferase* (*LUC*) reporter gene (Fig. 7b). Both SRG2 and SRG3 exhibited transcriptional repression activity and this activity was abolished by truncation of the EAR motif (Fig. 7c), which did not influence their localization (Fig. S5e–g).

It has been previously reported that NO may modulate the transcriptional repressive activity of SRG1 (Cui *et al.*, 2018). Therefore, we tested if NO might impact the transcriptional repressive activity of either SRG2 or SRG3. As expected, application of the NO donor, SNP, strikingly reduced the ability of SRG3 to operate as a transcriptional repressor. Surprisingly, and in complete contrast, NO was not found to blunt the transcriptional repressive activity of SRG2 following the addition of two distinct NO donors, SNP (Fig. 7d) and GSNO (Fig. 7e). In a *gsnor1-3* genetic background, which chronically accumulates (S)NO, SRG3-dependent transcriptional repression was abolished (Fig. 7f), which was not the case for SRG2-dependent transcriptional repression, which was slightly diminished. However, the chronic, long-term accumulation of (S)NO in the *gsnor1-3* line may result in the indirect action of these molecules on this activity. To determine if SRG function might be impacted by NO in *SRG* overexpression plants, we determined the NO concentration in these lines. The concentration of NO accumulation in these plants was similar to that of the wild-type line (Fig. S6). Collectively, our findings show that, remarkably, SRG2 and SRG3, despite their high degree of sequence similarity, were differentially regulated by direct NO function.

NO selectively *S*-nitrosylates SRG proteins

S-nitrosylation is a key mechanism to convey NO bioactivity (Astier *et al.*, 2011; Yu *et al.*, 2012). As our data suggest that NO can directly inhibit SG3 but not SRG2 transcriptional repression activity, we determined if either SRG2 or SRG3 could be directly modified by NO. We generated recombinant SRG2 and SRG3 proteins using a MBP fusion protein system (MBP-SRG2 and MBP-SRG3, respectively) and exposed these proteins to the natural NO donors, GSNO (Fig. 8a) or Cys-NO (Fig. 8b) and monitored their possible *S*-nitrosylation by the BSA. No SRG2-SNO formation was detected by either GSNO or Cys-NO treatment *in vitro* (Fig. 8a,b), even following long film exposure times to detect weak signals (Fig. S7). By contrast, MBP-SRG3 was *S*-nitrosylated strongly in response to both GSNO and Cys-NO (Fig. 8a,b). In order to confirm and extend these findings, MBP-SRG2 and MBP-SRG3 were subjected to a range of GSNO concentrations and possible SNO formation determined. In agreement with our previous data, SRG3 was *S*-nitrosylated and, further, this redox-based PTM occurred in a GSNO concentration-dependent fashion (Fig. 8d). However, formation of SRG2-SNO could not be detected, even over a range of GSNO concentrations (Fig. 8c). Together, these data suggest that NO selectively modifies SRG proteins *in vitro*.

To determine if either SRG2 or SRG3 could be *S*-nitrosylated *in vivo*, we generated C-terminal *FLAG*-tagged *SRG2* (*SRG2-FLAG*) and *SRG3* (*SRG3-FLAG*), respectively. Subsequently, *Arabidopsis* protoplasts expressing the indicated transgene were exposed to GSNO and endogenous proteins subjected to the BSA. Subsequently, biotinylated proteins were purified with streptavidin beads. These proteins were then immunoblotted with an anti-FLAG antibody. SRG3 was found to be *S*-nitrosylated *in vivo*. By contrast, no *S*-nitrosylation of SRG2 could be detected (Fig. 8e). We next tested possible *S*-nitrosylation of SRG2 and SRG3 in *gsnor1-3* plants, which show increased concentrations of GSNO accumulation and, by extension, elevated levels of global SNO-protein formation. The BSA assay revealed the formation of SRG3-SNO. Conversely, no SRG2-SNO was detected (Fig. 8f). These data suggest that SRG3 but not SRG2 can be *S*-nitrosylated *in vivo* in a *gsnor1-3* genetic background.

We next investigated if SRG3-SNO formation or *S*-nitrosylation of SRG2 occurred during attempted pathogen infection. Following *Pst* DC3000 inoculation, SRG3-SNO formation was detected from 6 hpi (Fig. 8h). By contrast, SRG2-SNO could not be detected at any of the time points tested (Fig. 8g,h). Collectively, these findings imply that SRG3 but not SRG2 is the target of *in vitro* and *in vivo S*-nitrosylation.

To further explore the possible impact of increased SNO concentrations on phenotypes resulting from *SRG* overexpression,

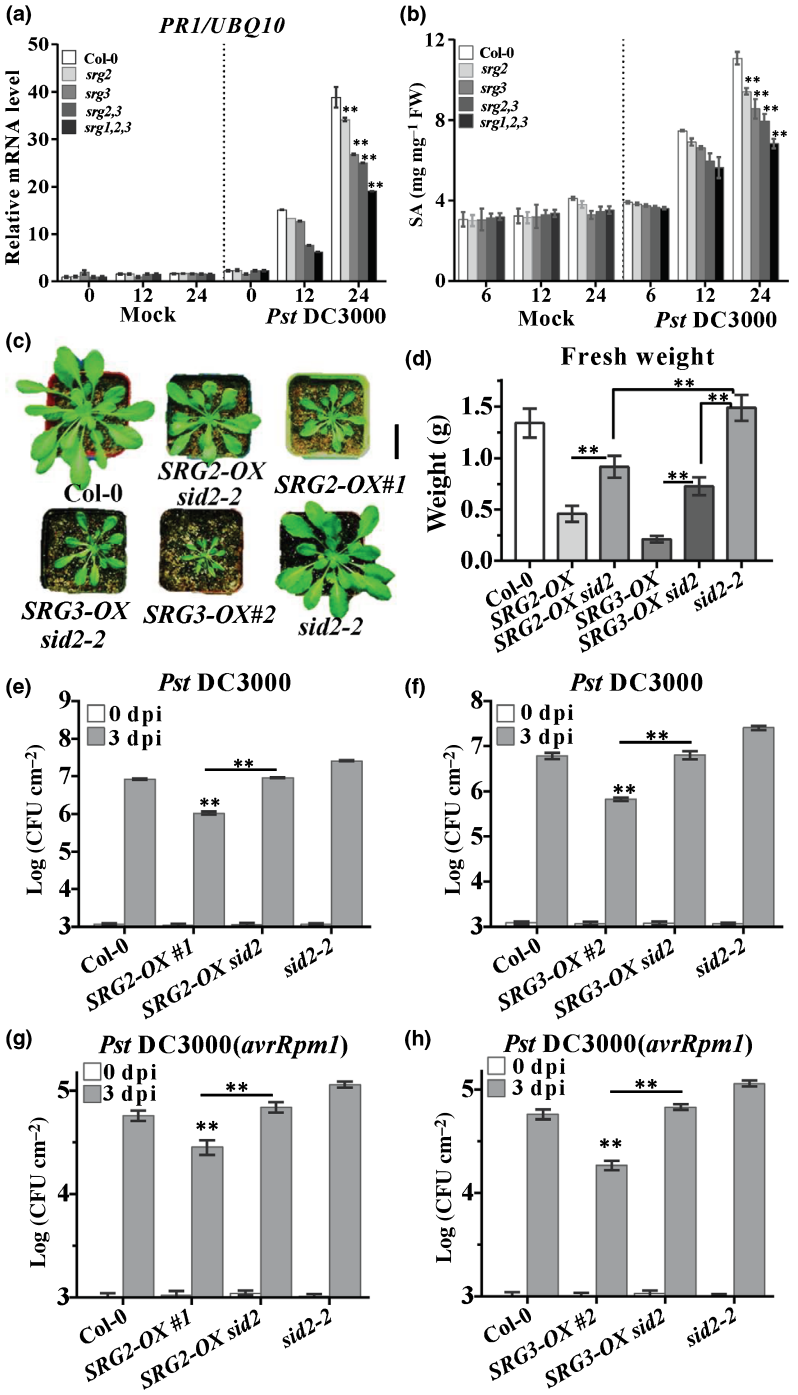

Fig. 6 *Arabidopsis SRG2* and *SRG3* function in salicylic acid (SA)-dependent signalling and immunity. (a) mRNA level of *PR1* in the given plant genotypes following pathogen challenge. Six-week-old plants were inoculated as indicated, followed by quantitative PCR. *Pseudomonas syringae* pv. *tomato* (*Pst*) DC3000 was resuspended in 10 mM $MgCl_2$ and $MgCl_2$ was used as mock. Error bars indicate means ± SD from three independent biological replicates. **, $P < 0.01$ (significant difference compared with wild-type Col-0 by ANOVA assay). (b) Total salicylic acid (SA) concentrations in the indicated *Arabidopsis* lines in response to pathogen challenge. Six-week-old plants were challenged as indicated, and the SA concentration was subsequently analysed by high-performance liquid chromatography. Error bars indicate ± SD ($n = 3$). ANOVA assays were performed to determine significant differences compared with wild-type Col-0 at 24 h post inoculation (hpi). **, $P < 0.01$. (c) Morphological phenotypes of the indicated plant genotypes at 6 wk old under short-day conditions. Bar, 2 cm. (d) FW in the stated *Arabidopsis* lines at 6 wk old under short-day conditions (8 h : 16 h, light : dark). Error bars indicate means ± SD ($n = 8$). **, $P < 0.01$ (ANOVA assay). (e–h) The titre of *Pst* DC3000 (e, f) or *Pst* DC3000(*avrRpm1*) (g, h) was determined at 0 and 3 d post-inoculation (dpi) following infiltration of virulent *Pst* DC3000 (e, f) or avirulent *Pst* DC3000 carrying *avrRpm1* (g, h) (1×10^5 CFU ml^{-1}). Error bars indicate means ± SD ($n = 7$). **, $P < 0.01$ (ANOVA assay). All experiments were repeated at least three times.

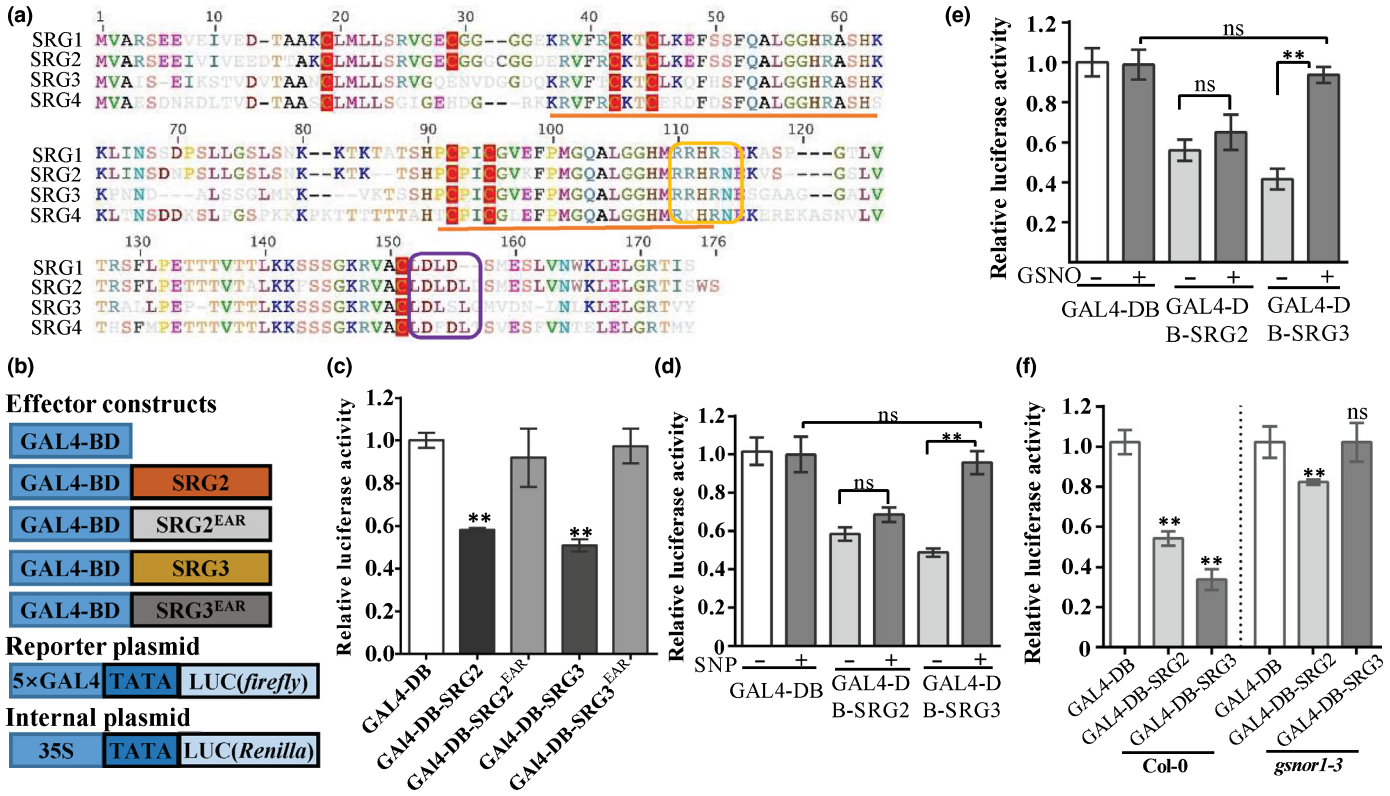

Fig. 7 Nitric oxide (NO) selectively modulates SRG transcriptional repression activity. (a) Protein sequence analysis of SRG2 and SRG3. Zinc finger (ZF) domains are indicated by orange lines. Nuclear localization signal (NLS) domain is highlighted by a yellow square. The ethylene-responsive element binding factor-associated amphiphilic repression (EAR) domain is indicated by a purple square. (b) Gene constructs of reporters and effectors used for transient transcriptional repressive activity assays. Reporter plasmids: 5 × GAL4 DNA binding sites were fused to the firefly luciferase (LUC) reporter gene. The CaMV*35S* promoter drives expression of renilla LUC functions as an internal control. Effector plasmids: the CaMV*35S* promoter is located upstream of either the GAL4 DNA-binding domain (GAL4- BD), a GAL4-BD-SRG2/3 fusion or a SRG2/3 EAR domain truncated mutant GAL4-DB-SRG2^{EAR}/3^{EAR} fusion. (c) Transient transcriptional repression assay. Indicated effector constructs were cotransformed into *Arabidopsis* protoplasts with reporter and internal control plasmids. Relative luciferase activity was quantified. Relative luciferase activities of fusion constructs compared with GAL4-DB control. Error bars represent means ± SD ($n = 10$). Experiments were repeated three times with similar results. **, $P < 0.01$. (d, e) Transient transcriptional repression assay after addition of NO donors, 10 mM sodium nitroprusside (SNP) (d) or 0.5 mM S-nitrosoglutathione (GSNO). Relative luciferase activity of GAL4-DB control was normalized as 1. Error bars represent means ± SD ($n = 10$). Experiments were repeated three times with similar results. **, $P < 0.01$; ns, not significant. (f) Transient transcriptional repression assay in wild-type Col-0 and *gsnor1-3* protoplasts. Relative luciferase activity of the GAL4-DB control was normalized as 1. Error bars represent means ± SD ($n = 10$). Experiments were repeated three times with similar results. **, $P < 0.01$ (significant difference compared to GAL4-DB by ANOVA assay).

we crossed *SRG2-OX* and *SRG3*-OX lines with *gsnor1-3* plants. *SRG3-OX#1 gsnor1-3* plants resembled the *gsnor1-3* line in terms of stature (Fig. 9a) and FW (Fig. 9b). However, *gsnor1-3* only partially suppressed the growth phenotype of the *SRG2-OX#1* line (Fig. 9a,b). Further, leaf infiltration of *Pst* DC3000 revealed that *SRG3-OX#1 gsnor1-3* plants supported an increased titre of bacteria relative to *SRG2-OX#1 gsnor1-3* plants (Fig. 9c,d). In aggregate, increased SNO concentrations in *gsnor1-3* plants abolished *SRG3*-dependent disease resistance but not *SRG2-OX#1* mediated protection.

Discussion

Our findings show that SRG2 and SRG3 function as transcriptional repressors, presumably through the recruitment of the corepressor, TOPLESS, via interaction with their EAR domain, in a similar fashion to SRG1 (Cui *et al.*, 2018). Further, SRG3 was *S*-nitrosylated *in vitro* by both Cys-NO and GSNO, two natural NO donors, and *in vivo* in response to attempted pathogen infection. Also, following (S)NO accumulation and subsequent SRG3 *S*-nitrosylation, the transcriptional repressive activity of SRG3 was abolished. In addition, *gsnor1-3*, which results in increased total cellular (S)NO accumulation, suppressed the growth and immunity phenotypes associated with ectopic overexpression of *SRG3* in *SRG3-OX gsnor1-3* lines. Remarkably, SRG2 was not *S*-nitrosylated either *in vitro* or in *vivo* following attempted pathogen infection. It was also surprising that (S)NO accumulation failed to directly abolish the transcriptional repressive activity of SRG2. Moreover, *gsnor1-3* did not fully suppress the growth and immunity phenotypes associated with ectopic overexpression of *SRG2*. In aggregate, our results show that SRG C2H2 ZnTFs exhibit differential capacities to act as substrates for NO-mediated *S*-nitrosylation. Thus, while SRG1 and SRG3 undergo SNO formation, which regulates their biological

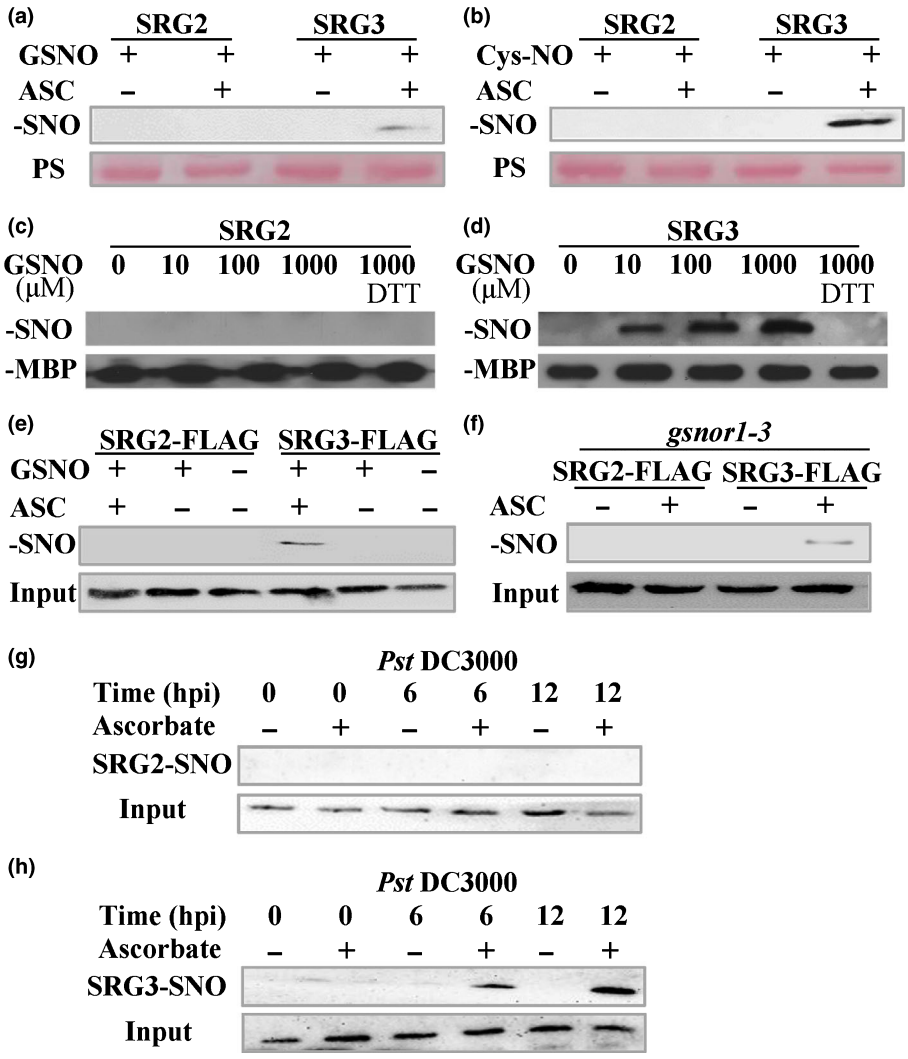

Fig. 8 Differential *S*-nitrosylation of SRG2 and SRG3. (a–d) *S*-nitrosylation analysis of SRG2 and SRG3 *in vitro*. Recombinant SRG2 and SRG3 proteins were generated using the myelin basic protein (MBP) expression system (MBP-SRG2 and MBP-SRG3, respectively). (a, b) The resulting SRG proteins were exposed to either 0.5 mM S-nitrosoglutathione (GSNO) (a) or 0.5 mM Cys-NO (b) with or without ascorbate (ASC) for monitoring *S*-nitrosylation of these proteins by the biotin switch assay (BSA). (c, d) Dose-dependent GSNO-dependent *S*-nitrosylation. PS, Ponceau staining; SNO, detection of *S*-nitrosothiol formation; -MBP, detection of MBP antibody as loading control. (e, f) *S*-nitrosylation of SRG2 and SRG3 *in vivo*; total protein extracts from *SRG2-FLAG* or *SRG3-FLAG* constructs in Col-0 plants (e) or *gsnor1-3* plants (f) were subjected to the BSA. Ten percent of total protein before BSA was used as input and detected by an anti-FLAG antibody; 0.5 mM GSNO was used in (e). (g, h) *Pseudomonas syringae* pv. *tomato* (*Pst*) DC3000 induced *S*-nitrosylation of SRG3 (h) but not SRG2 (g). Total protein extracts from *Arabidopsis* protoplast expressing SRG-FLAG constructs were subjected to the BSA after *Pst* DC3000 inoculation. Ascorbate was employed as indicated to control for SNO formation. Ten percent of total protein before BSA was used as input and detected by anti-FLAG.

function, the closely related family member, SRG2, is not a substrate for this redox-based PTM and is therefore, by extension, not regulated by this modification. Thus, the SRG family of C2H2 ZnTFs, despite their high similarity, are, remarkably, differentially regulated by NO bioactivity. Collectively, our findings support a model that is presented and described in Fig. 10.

By employing a molecular modelling strategy, we established that in both SRG1 and SRG3, Cys87, a highly conserved target residue for SNO formation (Cui *et al.*, 2018), is completely solvent exposed and fully accessible for modification by NO. Conversely, in SRG2, Cys87 is significantly less accessible to NO-driven *S*-nitrosylation (Fig. S8a–j). Thus, our data suggest that the observed differential *S*-nitrosylation of SRG proteins is facilitated by the structural location of Cys87 within SRG2 relative to the position of this residue within SRG1 and SRG3. To the extent of our knowledge, this is the first report of a closely related protein family being differentially regulated by this redox-based modification in either plants or animals.

Differential regulation of a plant TF gene family by a given PTM has, for example, also been demonstrated for the basic leucine zipper TGA transcriptional activators which function in both plant immunity and development (Pontier *et al.*, 2002). This TF family consisting of 10 members has been proposed to bind TGACG-motifs in SA-regulated promoters from

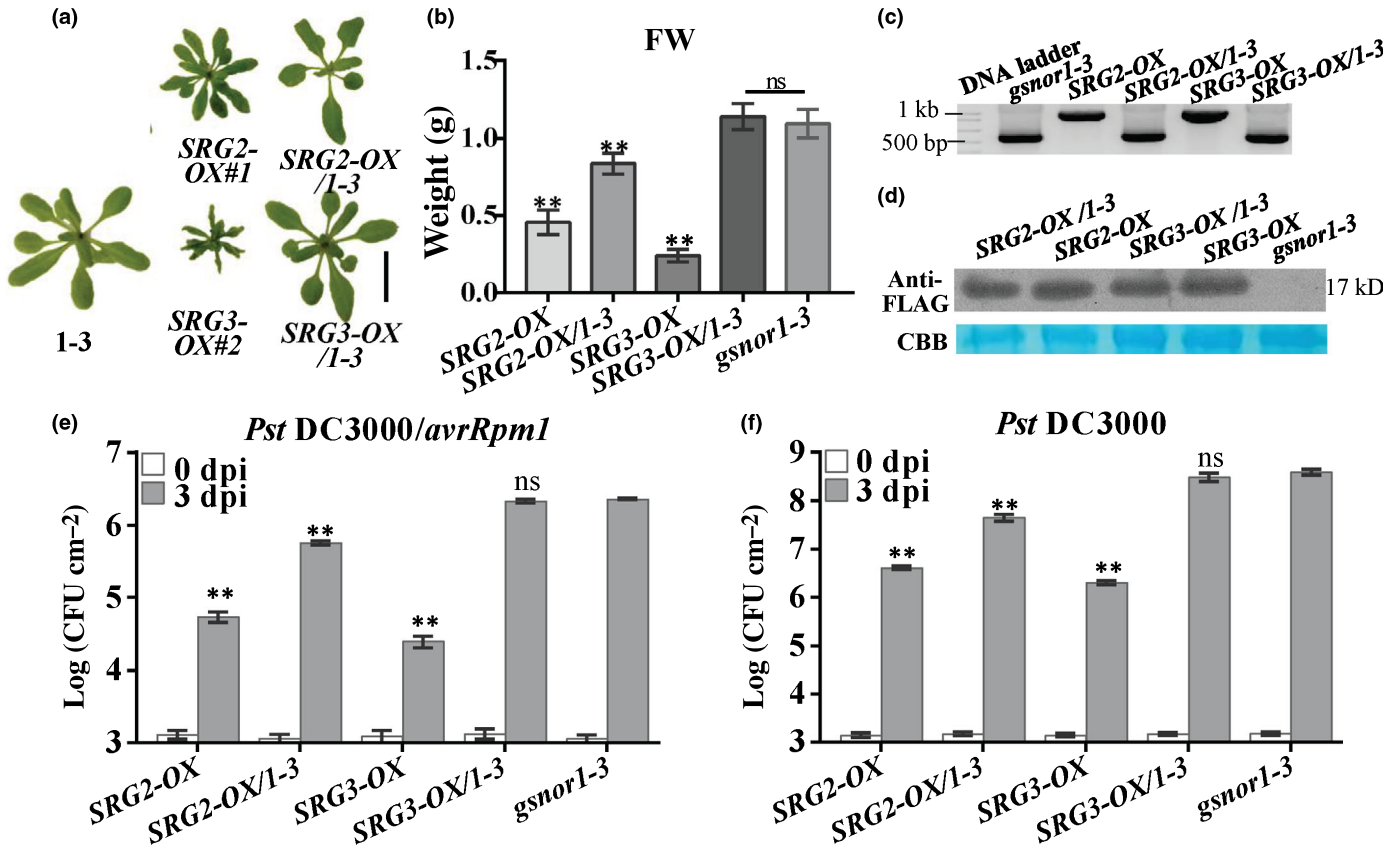

Fig. 9 *SRG* overexpression phenotypes are differentially suppressed by *gsnor1-3*. (a) Morphological phenotype of indicated genotypes of 6-wk-old plants grown under short-day conditions. Bar, 2 cm. (b) FW quantification of the stated 6-wk-old *Arabidopsis* lines grown under short-day conditions. Error bars indicate means ± SD ($n = 8$). **, $P < 0.01$; ns, not significant. (c) Genotyping analysis of the indicated plant lines. Specific primers for analysis of the T-DNA insertion site in *gsnor1-3* plants were employed to perform this experiment. (d) Detection of SRG protein expression in *SRG* overexpression (*SRG-OX*) lines. Western blot analysis was carried out to detect SRG proteins in the indicated plant lines using an anti-FLAG antibody. Coomasie Brilliant Blue (CBB) stain was employed as a loading control. (e, f) Titre of *Pseudomonas syringae* pv. *tomato* (*Pst*) DC3000(*avrRpm1*) (e) or *Pst* DC3000 (f) was determined at 0 and 3 d post-inoculation (dpi) in each indicated line. The concentration of bacteria used in these experiments was 1×10^5 CFU ml^{-1}. Error bars indicate means ± SD ($n = 7$). Experiments were repeated three times with similar results. **, $P < 0.01$; ns, not significant.

Arabidopsis and tobacco, which have been shown to be functionally relevant (Zhang *et al.*, 1999; Després *et al.*, 2000). Two TGA TFs are specifically targeted for developmental stage-specific proteolysis by the 26S proteasome, presumably following ubiquitination of a target lysine residue (Pontier *et al.*, 2002). Thus, TGA TFs may be regulated by differential targeted proteolysis, serving to modulate the contribution of specific members of this multigene TF family to complex developmental pathways.

To explore the differential *S*-nitrosylation of SRG proteins further, we undertook phylogenetic analysis to determine the possible selective pressure on *SRG1*, *SRG2* and *SRG3* (Methods S1, S2). This analysis suggested more nonsynonymous to synonymous substitutions, indicating the presence of positive selection (Table S2). Thus, the duplication of *SRG* genes may have resulted in subfunctionalization: the resulting gene copies post-duplication specialize to perform different functions within the same genetic pathway. Alternatively, neofunctionalization might have ensued, where one gene copy maintains the ancestral function while the additional copies are selected to perform novel activities outside the original genetic pathway. Our *SRG* functional data suggest that loss-of-function mutations in *SRG1*, *SRG2* or *SRG3* result in decreased disease resistance. Further, the negative impact on disease resistance of the *srg2 srg3* double loss-of-function mutant is additive relative to the *srg2* and *srg3* single loss-of-function mutants, implying that these genes may have evolved, at least partially, separate functions in the regulation of plant immunity. Further, the *srg1 srg2 srg3* triple loss-of-function mutant exhibits greater pathogen susceptibility relative to the *srg2 srg3* double loss-of-function mutant, indicating that all three *SRG* genes may have related but separable functions associated with plant immunity. Null loss-of-function mutations within the same genetic pathway would not be expected to be additive. These findings are therefore consistent with neofunctionalization of the *SRG* gene family, where one gene copy maintains the ancestral function, while the additional copies are selected to perform novel functions outside the original genetic pathway. Our experimental data also demonstrate that SRG1 and SRG3 are actively *S*-nitrosylated and this redox-based PTM regulates the activity of these proteins. By contrast, SRG2 is not subject to SNO formation. This feature also clearly differentiates SRG proteins at the molecular level.

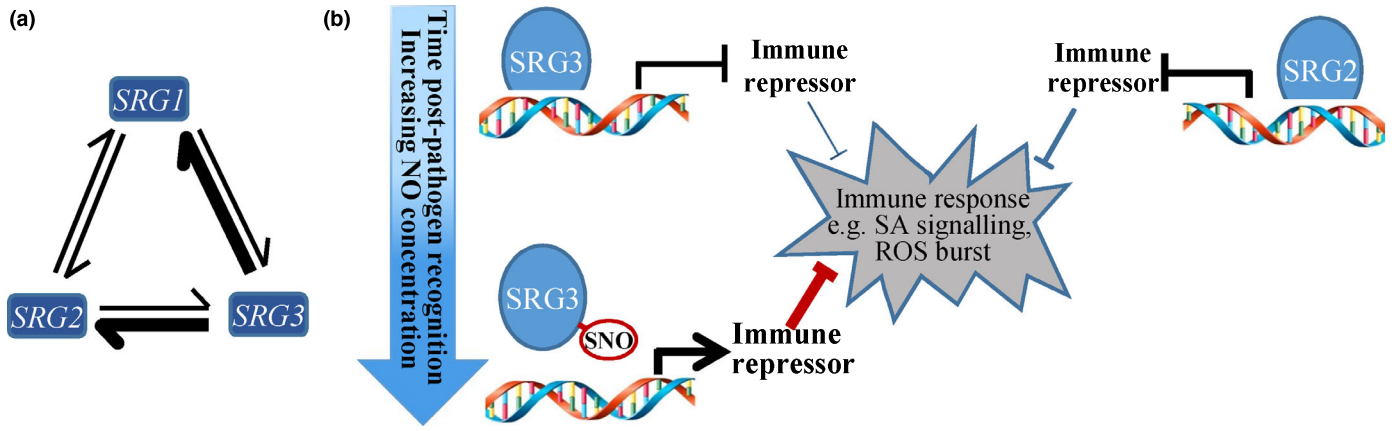

Fig. 10 Models showing SRG transcriptional and post-transcriptional regulation. (a) Schematic showing the reciprocal regulation of *SRG* gene expression by cognate SRG proteins. Arrows indicate the direction of action of given SRG proteins on the gene expression of other *SRG* family members. The weight of the arrows indicates the strength of a given action. (b) Model depicting the role of SRG proteins in plant immunity. Attempted pathogen infection rapidly triggers the nitrosative burst leading to nitric oxide (NO) production. The accumulation of NO drives the expression of selected *SRG* family members. This regulatory feature may occur through an indirect mechanism: *SRG* transcriptional repressors repress the transcription of a transcriptional repressor that targets *SRG* genes. SRG2 and SRG3 transcriptional repressors subsequently repress the transcription of a repressor of salicylic acid (SA) signalling and reactive oxygen species (ROS) accumulation, contributing to the establishment of plant immunity. As the concentration of NO accumulates over time, SRG3 becomes *S*-nitrosylated, resulting in a structural change precluding binding of SRG3 to its cognate *cis*-element. Thus, the transcriptional repressive activity of SRG3 is abolished, enabling expression of immune repressor(s) that contribute to the damping of the defence response. By contrast, NO does not drive the expression of *SRG2*, which is induced by other defence-related cues. Remarkably, SRG2 is not sensitive to direct NO-mediated *S*-nitrosylation. Thus, the SRG family of C2H2 ZnTFs, despite their high similarity, are differentially regulated by NO bioactivity.

The evolution of transcriptional regulatory networks has been proposed to occur predominantly through variation in *cis*-regulatory elements located within the promoters of target genes (Sorrells *et al.*, 2015; Sorrells & Johnson, 2015). This is because mutations in transcription factors would potentially result in widespread consequences relative to mutations within the regulatory elements themselves. Conversely, the accumulating data imply that variations in transcriptional regulators themselves can also drive the evolution of complex transcriptional regulatory networks, supported through gene duplication events of cognate transcriptional activators (Force *et al.*, 1999; Innan & Kondrashov, 2010). We suggest that the plant SRG family of C2H2 ZnTFs represents a quintessential example of this type of transcriptional-network evolution.

Interestingly, our results suggest that all members of the *SRG* family of ZnTFs reciprocally regulate the transcription of other members of this gene family. Thus, loss-of-function mutations in *SRG1*, *SRG2* or *SRG3* impact the associated transcript accumulation of the other two *SRG* genes. For example, direct comparison of *SRG* transcript abundances shows that loss of *SRG3* function results in *c.* 80% reduction in transcript accumulation for *SRG2* and a 70% reduction for *SRG1*. These data establish *SRG3* as the SRG family member that has the greatest influence on the expression of other *SRG* genes. Analysis of the promoter sequences associated with *SRG* genes reveals, in each case, multiple potential binding motifs for C2H2 ZnTFs. Therefore, it is possible that the observed reciprocal regulation of mRNA abundance amongst *SRG* family members is mediated through the direct binding of a given SRG TF to cognate *cis*-elements within the promoter sequences of other *SRG* genes. However, our data suggest that SRG1, SRG2 and SRG3 function as transcriptional repressors and hence mutations in these TFs would be expected to increase rather than decrease the transcript abundance of other *SRG* family members. Thus, the observed reciprocal regulation of gene expression amongst *SRG* family members may not occur through direct promoter binding and subsequent transcriptional regulation. More likely, our data infer that *SRG* reciprocal regulation occurs indirectly, perhaps by the given SRG repressing the transcription of a transcriptional repressor, which would ordinarily target other *SRG* family members.

Reciprocal regulation of gene expression is typically linked to feedback loops. A classic example is the circadian clock where the basic molecular architecture consists of negative-feedback loops where positive and negative components control each other's expression to generate oscillations with an approximate 24 h period (Bell-Pedersen *et al.*, 2005). In this context, the first described feedback loop of the *Arabidopsis* circadian clock was based on the reciprocal regulation between TIMING OF CAB EXPRESSION 1 (TOC1) and CIRCADIAN CLOCK-ASSOCIATED 1 (CCA1)/LATE ELONGATED HYPOCOTYL (LHY). CCA1 and LHY are Myb TFs that bind directly to the TOC1 promoter to negatively regulate its expression, while TOC1 binds directly to the CCA1 and LHY promoters negatively regulating their expression (Gendron *et al.*, 2012). The molecular mechanism underpinning SRG reciprocal regulation would therefore be an interesting target for future investigation, especially because, unlike the plant circadian clock example, SRG reciprocal regulation is likely to be indirect and also there is a general paucity of information on similar molecular interactions in plants.

Acknowledgements

BC and QP were supported by a China Scholarship Council (CSC) scholarship. QP was subsequently funded by the Natural Science Foundation of Jiangsu Province of China (SBK2017040656) and the National Natural Science Foundation of China (31700241). DF was funded by an award from the Daphne Jackson Trust together with the University of Edinburgh. This work was supported by a Biotechnology and Biological Sciences Research Council (BBSRC) research grant BB/DO11809/1 to GJL. We thank Nottingham *Arabidopsis* Stock Centre for providing seeds of *Arabidopsis* mutants. We also would like to thank Dr Jianru Zuo (Institute of Developmental Biology and Genetics, China) and Dr Chengcai Chu (Institute of Developmental Biology and Genetics, China) for sharing vectors for the chemical transcriptional induction system and transcriptional repressive activity assay, respectively.

Author contributions

BC, QP and GJL formulated the experimental strategy. QP, BC, DF, YL, SX, SU, BY and JJ performed experiments. QP, BC, FL, and GJL wrote the paper.

ORCID

Beimi Cui https://orcid.org/0000-0002-4901-1988
Fengquan Liu https://orcid.org/0000-0001-9325-1500
Gary J. Loake https://orcid.org/0000-0002-7989-9180
Qiaona Pan https://orcid.org/0000-0002-9142-1905

References

Astier J, Besson-Bard A, Lamotte O, Bertoldo J, Bourque S, Terenzi H, Wendehenne D. 2012. Nitric oxide inhibits the ATPase activity of the chaperone-like AAA+ ATPase CDC48, a target for *S*-nitrosylation in cryptogein signalling in tobacco cells. *Biochemical Journal* **447**: 249–260.

Astier J, Rasul S, Koen E, Manzoor H, Besson-Bard A, Lamotte O, Jeandroz S, Durner J, Lindermayr C, Wendehenne D. 2011. *S*-nitrosylation: an emerging post-translational protein modification in plants. *Plant Science* **181**: 527–533.

Bellin D, Asai S, Delledonne M, Yoshioka H. 2013. Nitric oxide as a mediator for defense responses. *Molecular Plant–Microbe Interactions* **26**: 271–277.

Bell-Pedersen D, Cassone VM, Earnest DJ, Golden SS, Hardin PE, Thomas TL, Zoran MJ. 2005. Circadian rhythms from multiple oscillators: lessons from diverse organisms. *Nature Reviews Genetics* **6**: 544–556.

Chen K, Chen L, Fan J, Fu J. 2013. Alleviation of heat damage to photosystem II by nitric oxide in tall fescue. *Photosynthesis research* **116**: 21–31.

Chen R, Sun S, Wang C, Li Y, Liang Y, An F, Li C, Dong H, Yang X, Zhang J. 2009. *The Arabidopsis PARAQUAT RESISTANT2* gene encodes an *S*-nitrosoglutathione reductase that is a key regulator of cell death. *Cell Research* **19**: 1377–1387.

Clough SJ, Bent AF. 1998. Floral dip: a simplified method for *Agrobacterium*-mediated transformation of *Arabidopsis thaliana*. *The Plant Journal* **16**: 735–743.

Corpas FJ, Barroso JB. 2014. Peroxisomal plant nitric oxide synthase (NOS) protein is imported by peroxisomal targeting signal type 2 (PTS2) in a process that depends on the cytosolic receptor PEX7 and calmodulin. *FEBS Letters* **588**: 2049–2054.

Cui B, Pan Q, Clarke D, Villarreal MO, Umbreen S, Yuan B, Shan W, Jiang J, Loake GJ. 2018. *S*-nitrosylation of the zinc finger protein SRG1 regulates plant immunity. *Nature Communications* **9**: 4226.

Delledonne M, Xia Y, Dixon RA, Lamb C. 1998. Nitric oxide functions as a signal in plant disease resistance. *Nature* **394**: 585–588.

Delledonne M, Zeier J, Marocco A, Lamb C. 2001. Signal interactions between nitric oxide and reactive oxygen intermediates in the plant hypersensitive disease resistance response. *Proceedings of the National Academy of Sciences, USA* **98**: 13454–13459.

Després C, DeLong C, Glaze S, Liu E, Fobert PR. 2000. The Arabidopsis NPR1/NIM1 protein enhances the DNA binding activity of a subgroup of the TGA family of bZIP transcription factors. *Plant Cell* **12**: 279–290.

Earley KW, Haag JR, Pontes O, Opper K, Juehne T, Song K, Pikaard CS. 2006. Gateway-compatible vectors for plant functional genomics and proteomics. *The Plant Journal* **45**: 616–629.

Feechan A, Kwon E, Yun BW, Wang YQ, Pallas JA, Loake GJ. 2005. A central role for *S*-nitrosothiols in plant disease resistance. *Proceedings of the National Academy of Sciences, USA* **102**: 8054–8059.

Force A, Lynch M, Pickett FB, Amores A, Yan Y-l, Postlethwait J. 1999. Preservation of duplicate genes by complementary, degenerative mutations. *Genetics* **151**: 1531–1545.

Gendron JM, Pruneda-Paz JL, Doherty CJ, Gross AM, Kang SE, Kay SA. 2012. *Arabidopsis* circadian clock protein, TOC1, is a DNA-binding transcription factor. *Proceedings of the National Academy of Sciences, USA* **109**: 3167–3172.

Gómez-Gómez L, Felix G, Boller T. 1999. A single locus determines sensitivity to bacterial flagellin in *Arabidopsis thaliana*. *The Plant Journal* **18**: 277–284.

Grant JJ, Loake GJ. 2000. Role of reactive oxygen intermediates and cognate redox signaling in disease resistance. *Plant Physiology* **124**: 21–29.

Grant JJ, Yun BW, Loake GJ. 2000. Oxidative burst and cognate redox signalling reported by luciferase imaging: identification of a signal network that functions independently of ethylene, SA and Me-JA but is dependent on MAPKK activity. *The Plant Journal* **24**: 569–582.

Grant MR, Godiard L, Straube E, Ashfield T, Lewald J, Sattler A, Innes RW, Dangl JL. 1995. Structure of the Arabidopsis RPM1 gene enabling dual specificity disease resistance. *Science* **269**: 843–846.

Gupta KJ, Fernie AR, Kaiser WM, van Dongen JT. 2011. On the origins of nitric oxide. *Trends in Plant Science* **16**: 160–168.

Hussain A, Yun BW, Kim JH, Gupta KJ, Hyung NI, Loake GJ. 2019. Novel and conserved functions of *S*-nitrosoglutathione reductase (GSNOR) in tomato. *Journal of Experimental Botany* **70**: 4877–4886.

Innan H, Kondrashov F. 2010. The evolution of gene duplications: classifying and distinguishing between models. *Nature Reviews Genetics* **11**: 97–108.

Jabs T, Dietrich RA, Dangl JL. 1996. Initiation of runaway cell death in an *Arabidopsis* mutant by extracellular superoxide. *Science* **273**: 1853–1856.

Jaffrey SR, Snyder SH. 2001. The biotin switch method for the detection of *S*-nitrosylated proteins. *Science's STKE* **2001**: pl1.

Kagale S, Rozwadowski K. 2011. EAR motif-mediated transcriptional repression in plants: an underlying mechanism for epigenetic regulation of gene expression. *Epigenetics* **6**: 141–146.

Kim Y, Park S, Gilmour SJ, Thomashow MF. 2013. Roles of CAMTA transcription factors and salicylic acid in configuring the low-temperature transcriptome and freezing tolerance of *Arabidopsis*. *The Plant Journal* **75**: 364–376.

Kneeshaw S, Gelineau S, Tada Y, Loake GJ, Spoel SH. 2014. Selective protein denitrosylation activity of Thioredoxin-h5 modulates plant immunity. *Molecular Cell* **56**: 153–162.

Kwon E, Feechan A, Yun BW, Hwang BH, Pallas JA, Kang JG, Loake GJ. 2012. *AtGSNOR1* function is required for multiple developmental programs in *Arabidopsis*. *Planta* **236**: 887–900.

Lee U, Wie C, Fernandez BO, Feelisch M, Vierling E. 2008. Modulation of nitrosative stress by *S*-nitrosoglutathione reductase is critical for thermotolerance and plant growth in *Arabidopsis*. *Plant Cell* **20**: 786–802.

Lindermayr C, Sell S, Muller B, Leister D, Durnera J. 2010. Redox regulation of the NPR1-TGA1 system of *Arabidopsis thaliana* by nitric oxide. *Plant Cell* **22**: 2894–2907.

Mengel A, Ageeva A, Georgii E, Bernhardt J, Wu KQ, Durner J, Lindermayr C. 2017. Nitric oxide modulates histone acetylation at stress genes by inhibition of histone deacetylases. *Plant Physiology* **173**: 1434–1452.

Mengel A, Chaki M, Shekariesfahlan A, Lindermayr C. 2013. Effect of nitric oxide on gene transcription- *S*-nitrosylation of nuclear proteins. *Frontiers in Plant Science* **4**: 293.

Nakagawa T, Kurose T, Hino T, Tanaka K, Kawamukai M, Niwa Y, Toyooka K, Matsuoka K, Jinbo T, Kimura T. 2007. Development of series of gateway binary vectors, pGWBs, for realizing efficient construction of fusion genes for plant transformation. *Journal of Bioscience and Bioengineering* **104**: 34–41.

Oide S, Bejai S, Staal J, Guan N, Kaliff M, Dixelius C. 2013. A novel role of PR2 in abscisic acid (ABA) mediated, pathogen-induced callose deposition in *Arabidopsis thaliana*. *New Phytologist* **200**: 1187–1199.

Palmieri MC, Sell S, Huang X, Scherf M, Werner T, Durner J, Lindermayr C. 2008. Nitric oxide-responsive genes and promoters in *Arabidopsis thaliana*: a bioinformatics approach. *Journal Experimental Botany* **59**: 177–186.

Parani M, Rudrabhatla S, Myers R, Weirich H, Smith B, Leaman DW, Goldman SL. 2004. Microarray analysis of nitric oxide responsive transcripts in *Arabidopsis*. *Plant Biotechnology Journal* **2**: 359–366.

Pontier D, Privat I, Trifa Y, Zhou JM, Klessig DF, Lam E. 2002. Differential regulation of TGA transcription factors by post-transcriptional control. *The Plant Journal* **32**: 641–653.

Pyott DE, Sheehan E, Molnar A. 2016. Engineering of CRISPR/Cas9-mediated potyvirus resistanc in transgene-free *Arabidopsis* plants. *Molecular Plant Pathology* **17**: 1276–1288.

Smith JM, Heese A. 2014. Rapid bioassay to measure early reactive oxygen species production in *Arabidopsis* leave tissue in response to living *Pseudomonas syringae*. *Plant Methods* **10**: 6.

Sorrells TR, Booth LN, Tuch BB, Johnson AD. 2015. Intersecting transcription networks constrain gene regulatory evolution. *Nature* **523**: 361–365.

Sorrells TR, Johnson AD. 2015. Making sense of transcription networks. *Cell* **161**: 714–723.

Spadaro D, Yun BW, Spoel SH, Chu CC, Wang YQ, Loake GJ. 2010. The redox switch: dynamic regulation of protein function by cysteine modifications. *Physiologia Plantarum* **138**: 360–371.

Tada Y, Spoel SH, Pajerowska-Mukhtar K, Mou ZL, Song JQ, Wang C, Zuo JR, Dong X. 2008. Plant immunity requires conformational charges of NPR1 via S-nitrosylation and thioredoxins. *Science* **321**: 952–956.

Thordal-Christensen H, Zhang Z, Wei Y, Collinge DB. 1997. Subcellular localization of H_2O_2 in plants. H_2O_2 accumulation in papillae and hypersensitive response during the barley–powdery mildew interaction. *The Plant Journal* **11**: 1187–1194.

Torres MA, Jones JD, Dangl JL. 2006. Reactive oxygen species signaling in response to pathogens. *Plant Physiology* **141**: 373–378.

Wang YQ, Feechan A, Yun BW, Shafiei R, Hofmann A, Taylor P, Xue P, Yang FQ, Xie ZS, Pallas JA *et al.* 2009. *S*-nitrosylation of AtSABP3 antagonizes the expression of plant immunity. *Journal of Biological Chemistry* **284**: 2131–2137.

Whalen MC, Innes RW, Bent AF, Staskawicz BJ. 1991. Identification of Pseudomonas syringae pathogens of Arabidopsis and a bacterial locus determining avirulence on both Arabidopsis and soybean. *Plant Cell* **3**: 49–59.

Xu S, Guerra D, Lee U, Vierling E. 2013. S-nitrosoglutathione reductases are low-copy number, cysteine-rich proteins in plants that control multiple developmental and defense responses in Arabidopsis. *Frontiers in Plant Science* **4**: 430.

Yu MD, Lamattina L, Spoel SH, Loake GJ. 2014. Nitric oxide function in plant biology: a redox cue in deconvolution. *New Phytologist* **202**: 1142–1156.

Yu M, Yun B-W, Spoel SH, Loake GJ. 2012. A sleigh ride through the SNO: regulation of plant immune function by protein S-nitrosylation. *Current Opinion in Plant Biology* **15**: 424–430.

Yun BW, Feechan A, Yin MH, Saidi NBB, Le Bihan T, Yu M, Moore JW, Kang JG, Kwon E, Spoel SH *et al.* 2011. *S*-nitrosylation of NADPH oxidase regulates cell death in plant immunity. *Nature* **478**: 264–268.

Yun BW, Skelly MJ, Yin MH, Yu MD, Mun BG, Lee SU, Hussain A, Spoel SH, Loake GJ. 2016. Nitric oxide and *S*-nitrosoglutathione function additively during plant immunity. *New Phytologist* **211**: 516–526.

Zago E, Morsa S, Dat JF, Alard P, Ferrarini A, Inze D, Delledonne M, Van Breusegem F. 2006. Nitric oxide- and hydrogen peroxide-responsive gene regulation during cell death induction in tobacco. *Plant Physiology* **141**: 404–411.

Zhan N, Wang C, Chen L, Yang H, Feng J, Gong X, Ren B, Wu R, Mu J, Li Y *et al.* 2018. *S*-nitrosylation targets GSNO reductase for selective autophagy during hypoxia responses in plants. *Molecular Cell* **71**: 142–154.e6.

Zhang X, Henriques R, Lin S-S, Niu Q-W, Chua N-H. 2006. *Agrobacterium*-mediated transformation of *Arabidopsis thaliana* using the floral dip method. *Nature Protocols* **1**: 641.

Zhang Y, Fan W, Kinkema M, Li X, Dong X. 1999. Interaction of NPR1 with basic leucine zipper protein transcription factors that bind sequences required for salicylic acid induction of the *PR-1* gene. *Proceedings of the National Academy of Sciences, USA* **96**: 6523–6528.

Zuo J, Niu QW, Chua NH. 2000. An estrogen receptor-based transactivator XVE mediates highly inducible gene expression in transgenic plants. *The Plant Journal* **24**: 265–273.

Supporting Information

Additional Supporting Information may be found online in the Supporting Information section at the end of the article.

Fig. S1 Phylogenetic tree of C2H2 type zinc finger genes in *Arabidopsis*.

Fig. S2 Identification of *SRG* mutants.

Fig. S3 Loss of *SRG* function affects *Arabidopsis* cell death development and ROS.

Fig. S4 SA-related gene expression in *srg* mutants.

Fig. S5 *SRG2* and *SRG3* encode nuclear-located proteins.

Fig. S6 Determination of NO concentration in *SRG2* and *SRG3* overexpression lines.

Fig. S7 SRG2 is not *S*-nitrosylated in response to NO accumulation.

Fig. S8 Computational modelling reveals structural differences between SRG proteins.

Methods S1 SRG protein structure analysis.

Methods S2 Evolutionary analysis of *SRG* genes.

Table S1 Primer list.

Table S2 Evolutionary analysis of *SRG* genes.

Please note: Wiley Blackwell are not responsible for the content or functionality of any Supporting Information supplied by the authors. Any queries (other than missing material) should be directed to the *New Phytologist* Central Office.